SPIN POLARIZED CHARGE CARRIER INJECTION, TRANSPORT, AND DETECTION IN ORGANIC SEMICONDUCTORS

A DISSERTATION
SUBMITTED TO THE FACULTY OF THE GRADUATE SCHOOL
OF THE UNIVERSITY OF MINNESOTA

BY

MOHAMMAD YUNUS

IN PARTIAL FULFILLMENT OF THE REQUIREMENTS
FOR THE DEGREE OF
DOCTOR OF PHILOSOPHY

PROF. P. PAUL RUDEN, ADVISER

APRIL 2011

ACKNOWLEDGEMENTS

Many individuals deserve my thanks for their hard work, patience, and support all through the years of research represented by this thesis. I thank my advisor, Prof. Paul Ruden, for his continuous guidance and supervision throughout the progress of the work. My special recognition goes to Dr. Darryl Smith, our research collaborator at Los Alamos National Laboratory (New Mexico) for his insightful and fruitful comments. I would like to thank my fellow graduate students, Dr. Zahed Kauser, Dr. Dominic Schroepfer, and Mr. Isaiah Steinke for their interaction on a daily basis. Access to the facilities of the Minnesota Supercomputing Institute for Digital Simulation and Advanced Computation is gratefully acknowledged. Finally, I would like to express my appreciation to the National Science Foundation and the Department of Electrical and Computer Engineering (University of Minnesota) for financial support.

ABSTRACT

In this thesis we explore spin polarized charge carrier injection, transport, and detection in organic semiconductors. Device structures considered have one or more ferromagnetic contacts to the organic semiconductor, and the condition for which charge carrier injection from ferromagnetic contacts is strongly spin polarized is discussed. Spin injection into semiconductors can be greatly enhanced if the injection mechanism is spin selective, such as is the case for tunnelling from ferromagnetic contacts. By contrast, if the carrier injection is by thermionic emission or another process that does not depend on spin, the injection is only weakly spin polarized. To discuss spin transport and spin detection, we consider a unipolar organic spin valve consisting of an organic semiconductor layer sandwiched between two ferromagnetic contacts. The polarizations of the magnetic contacts can be parallel or anti-parallel. Spin and charge carrier transport in the organic semiconductor is described by spin dependent transport equations in drift-diffusion approximation and the spin detection process is through magneto-resistance. We discuss the impact of various degrees of spin relaxation in organic semiconductors on the spatial variation of the spin current and its effect on magneto-resistance. The spatial profile of the spin current inside the organic semiconductor depends not only on the spin

diffusion length but also on the alignment of the contact polarizations. However, the magneto-resistance decreases strongly with decreasing spin diffusion length.

Electron tunnelling from a ferromagnetic contact can have significant spin dependence because the spatial part of the electron wave function is different for the majority and minority spin states of the ferromagnetic contacts. The tunnelling process occurs from the ferromagnetic contact through an insulating layer into the organic semiconductor. The insulating layer is modeled first as an ohmic layer with spin dependent contact resistances. The effectiveness of spin dependent contact resistances on spin polarized injection and magneto-resistance is examined on the basis of a simple analytical model. We then model the insulating layer as a tunnel barrier with spin dependent rate equations. Both majority and minority spin electrons of the ferromagnetic contact tunnel through the insulating layer into the localized molecular states of the organic semiconductor at the semiconductor/insulator interface. Tunnelling matrix elements and transition rates of the two spin types are calculated using a Transfer Hamiltonian approach. The transition rates are thus spin dependent and used in rate equations to calculate the injected (extracted) current for carriers of either spin direction. We explore the various aspects of the ferromagnetic contacts, the thickness and barrier height of the insulating layer, and the energy of the localized molecular states on spin injection and magneto-resistance. Consistent with the experimental data, the spin

injection from ferromagnetic contacts can be either positive or negative, and the magneto-resistance decreases strongly with the applied bias across the device.

TABLE OF CONTENTS

LIST OF TABLES

LIST OF FIGURES

LIST OF ABBREVIATIONS

OLED	Organic light emitting diode
FET	Field effect transistor
LED	Light emitting diode
RTD	Resonant tunnelling diode
FM	Ferromagnetic
LSMO	$La_{0.7}Sr_{0.3}MnO_3$
MR	Magneto-resistance
P	Parallel
AP	Anti parallel
SU	Spin up
SD	Spin down

Chapter 1

Introduction

Organic spintronics is a nascent but rapidly growing field where organic semiconductors are used to conduct and control a spin polarized current to increase device functionality. Certain π-conjugated polymers and crystals of relatively small hydrocarbon molecules – known as organic semiconductors – have in recent years become viable materials for electronic, optoelectronic, and photovoltaic devices.[1,2] These materials have processing advantages over conventional semiconductors for low-cost, large-area, and flexible device applications. Displays based on organic light emitting diodes (OLEDs) are already seeing commercial use.[3] Organic photovoltaic devices are also competing in existing commercial applications[4] and considerable improvements have already been achieved in the field of organic field effect transistors.[5] On the other hand, spintronics is a set of ideas that utilize spin (instead of, or in addition to charge) as the physical information carrying quantity. Commercial success of metal based spintronic devices has been achieved with recording heads and magnetic memories that use the giant magneto-resistance and tunneling magneto-resistance effects in so-called spin valves.[6,7]

Based on the success of metallic spintronics, intense research efforts are now devoted to include the spin degree of freedom into the realm of semiconductors. Key requirements for success in this effort include the following: efficient injection of spin polarized charge carriers through one device terminal; efficient transport and sufficiently long spin relaxation times within the host semiconductor material; effective control/manipulation of the spin polarized carriers in the structure (e.g., by using a gate bias) to provide the desired functionality; and effective detection of the spin polarized carriers at a second device terminal. Coupling the spin degree of freedom with electronic

devices could ultimately increase considerably the functionality and performances of semiconductor devices.[8,9,10] A number of spintronic device concepts, such as the spin polarized field effect transistor[11] (spin FET), spin polarized light emitting diode[12,13] (spin LED), and spin dependent resonant tunnelling diode[14](spin RTD) have been discussed in the literature, and some degree of success has been realized with each of these devices. In all of them, the semiconductors are inorganic materials. Spintronic devices based on organic semiconductors have also been reported recently.[15,16] The prospect of introducing spintronics into organic semiconductor technology could make the development of resistive memories and sensors based on organic semiconductors possible.[17]

1.1 Literature review

To date, very few theoretical works have been carried out on organic spintronics. The experimental situation is also not yet well established. However, there has been considerable progress, both theoretically and experimentally, in understanding the electron spin physics in inorganic semiconductors. In order to understand the spin dependent processes in organic semiconductors, we will apply the recent progress made in inorganic semiconductors to organic materials. Hence, this literature review will consist of works focusing on inorganic and organic semiconductors.

An essential requirement for spintronic device operation is efficient electrical spin injection into semiconductors. Though ferromagnetic (FM) contacts are spin polarized, Schmidt et al.[18] revealed that the large conductivity mismatch between FM contacts and semiconductors effectively suppresses spin injection. For the diffusive transport regime, they showed that the spin injection coefficient γ is proportional to σ_{SC}/σ_{FM}, where σ_{SC} and σ_{FM} are the conductivities of the semiconductor and the FM contact. Since $\sigma_{SC} << \sigma_{FM}$, the spin injection coefficient is always much less than unity. However, E. I. Rashbha[19] showed that a spin selective tunnel contact at the FM/semiconductor interface can solve the conductivity mismatch problem and greatly enhance spin injection from FM

contacts into semiconductors. The magnitude of the tunnel contact resistance should be of the order of the resistance of the semiconductor. D.L. Smith and R. N. Silver,[20] and J. D. Albrecht and D.L. Smith[21] also showed that a tunnel contact can facilitate spin injection into semiconductors. They calculated spin injection from FM contacts into semiconductors with different conductivities. They showed that spin injection into semiconductors increases with increasing conductivity of the semiconductor for a fixed tunnel contact. Electron tunnelling from a FM metal contact is spin dependent because the spatial part of the electron wave function is different for majority and minority spin states near the Fermi surface. In a device model this process can be effectively described by contact resistances that are different for majority and minority spin electrons. The effects of such spin injection modeled by spin dependent contact resistances have been discussed in the literature.[22,23,24,25] All these calculations have shown that spin dependent contact resistances can effectively inject spin polarized charge carriers into semiconductor materials.

Once the mechanism of efficient spin injection into a semiconductor material had been established, spin injection and detection from FM contacts were successfully demonstrated in inorganic semiconductors.[26,27,28,29,30,31] A FM metal contact usually forms a Schottky contact with the semiconductor. The experimental devices use a precise doping profile in the semiconductor near the FM interface in order to achieve a thin depletion layer. Tunnelling through the depletion region provides spin injection into these devices. The most studied material among the inorganic semiconductors has been gallium arsenide (GaAs). GaAs provides some favorable spin dependent optical properties that can be used to detect spin polarized electron injection. Spin dependent optical probes based on selection rules have been applied in demonstrating electrical spin injection, transport, and detection experimentally.[32] Unfortunately, these selection rules are not applicable in organic semiconductors. This makes spin experiments in organic semiconductors difficult. Efforts to detect spin injection in these latter materials therefore have focused on the measurement of the magneto-resistance of organic spin valves.

Organic semiconductors consist of π-conjugated hydrocarbons in which the valence states are formed primarily from bonding combinations of π-orbitals centered on carbon atoms and conduction states are formed primarily from the corresponding anti-bonding combinations of the π-orbitals. Typically these materials are highly disordered and their electronic states are not labelled by a wave vector. Conduction in most cases occurs by electron or hole hopping rather than by band transport, as described by the Boltzmann Transport Equation. As a result, carrier mobilities are much smaller in magnitude and stronger functions of carrier density and electric field strength than in inorganic semiconductors. They are generally undoped and essentially free of mobile charge carriers in equilibrium. Electrons and holes are introduced into the semiconductor by injection from metallic contacts. Low-work-function metals (such as aluminum or calcium) can be used to inject electrons and high-work-function metals (such as gold or platinum) can be used to inject holes in devices fabricated from organic semiconductors.[33,34] Because the principal elements making up most organic semiconductors (hydrogen and carbon) are very light, the spin orbit interaction in these materials is weak.[35] The hyperfine interaction due to the spin-1/2 hydrogen nuclei may play a significant role in some of the magneto-resistance phenomena observed with organic semiconductors,[36,37] and it may also provide the dominant relaxation mechanism for spin polarized carrier transport. However, this may vary from material to material as electron spin resonance experiments with certain organic molecules have yielded linewidths that are quite narrow,[38] consistent with the general notion that spin relaxation times in these materials are rather long.[39] Recent experiments in which hydrogen was replaced by deuterium in certain polymers have shed much light on this issue and have shown that large spin diffusion lengths are indeed attainable.[40] In contrast to inorganic semiconductors where the natural barrier formed by the depletion region was used to inject spin polarized charge carriers, a molecular monolayer grown by self assembly techniques to control the charge carrier injection[41,42] can be used as the tunnel layer to inject spin polarized charge carriers into organic semiconductors. The potential for integrating organic semiconductors with extremely spin polarized colossal magneto-resistance manganates, for example $La_{0.7}Sr_{0.3}MnO_3$ (LSMO), provides additional potential for organic spintronics.

Spin injection into organic semiconductors was first demonstrated by V. Dediu et al.[43] They used a device structure consisting an organic semiconductor sandwiched between two FM contacts; this device structure is referred to as an organic spin valve. They measured the magneto-resistance (MR) of an LSMO/T_6 (sexithienyl)/LSMO structure. Here MR represents the change of the resistance of the device structure as a result of applied magnetic field (i.e the resistance of the structure with applied magnetic field minus the resistance of the structure without magnetic field). The application of a magnetic field aligns the contact magnetizations, and the resultant MR is attributed to spin injection and transport in the T_6. The evidence of MR effects in organic spin valves was verified by Z. H. Xiong et al.[44,45] They used two different FM contacts (LSMO and cobalt) in an organic (8-hydroxy-quinoline aluminum, known as Alq_3) spin valve. Since the coercive magnetic field is different for LSMO and cobalt, the change of the contact magnetization will occur at different magnetic fields. As a result parallel (P) and anti-parallel (AP) alignments of the contact magnetizations will form depending on the applied magnetic field. For a particular applied bias across the device, the resistance of the organic spin valve changes when the alignment of the contacts changes from P to AP configuration, and a MR loop was found in their experiments. A change in the contact polarizations results in a change of the resistance of the device structure. This experiment clearly established spin injection and transport in organic semiconductors. Since the organic semiconductor layer thicknesses were much larger than tunnel lengths, carrier transport in the organic semiconductor was assumed to be diffusive, and the observed MR was not attributed to tunnelling from one contact to the other. These results were followed by successive evidence of MR effects in organic spin valves.[46,47,48,15,40] All these experiments have shown that organic semiconductors are suitable for spintronic applications.

A theoretical model of spin injection and transport in organic semiconductors was reported by P. P. Ruden and D. L Smith.[49] They showed that spin dependent contact resistances can effectively inject spin polarized electrons into organic semiconductors consistent with the theoretical model in inorganic semiconductors.[22, 23,24,25] They also showed that the voltage drop across a FM contact biased to collect spin polarized

electrons from the semiconductor will be measurably different for P and AP alignment of the contact polarizations, and thus this difference in voltage can be used to detect the spin polarized current.

1.2 Objective of this work

Organic semiconductors have been shown to be promising materials for next generation electronic, optoelectronic, and photovoltaic devices. In addition, the MR phenomena discussed in the literature demonstrated that organic semiconductors are also suitable for spintronic applications. The prospect of introducing spintronics into organic semiconductors could ultimately increase the performance of some devices already made from organic semiconductors. For example, we reported model results that show how spin polarized injection affects the formation and distribution of (emissive) singlet excitons.[50] Development of resistive memories and sensors are perhaps also possible using organic spintronics.[15,16,17] To characterize these devices, a sound understanding of spin polarized charge carrier injection, transport, and detection in organic semiconductors is indispensable.

Not much theoretical work so far has been done to understand spin injection and transport in organic semiconductors. When Z. H. Xiong et al. reported the giant MR effects in organic valves, the results prompted considerable debate in the scientific community. The initial experimental results suffered from a lack of reproducibility.[51] Some of the experimental results found for organic spin valves are puzzling. The observed magneto-resistances are either positive or negative and strongly decrease with the applied bias. Therefore, to understand the experimental results, a comprehensive theoretical study has become essential. This thesis serves the above purpose.

In this thesis, we report a comprehensive study of spin injection from FM contacts into organic semiconductors, transport of the injected spin through the organic semiconductors, and detection of the resultant spin through an extracting contact. First

we discuss spin injection from FM contacts into organic semiconductors. Tunnelling provides spin selectivity to inject spin polarized carriers into organic semiconductors. The tunnelling process occurs from the ferromagnetic contact through an insulating layer into the organic semiconductor. The insulating layer is modeled first by an ohmic layer with spin dependent contact resistances, and then by a tunnel layer with spin dependent rate equations. Spin and charge carrier transport in the organic semiconductor is described by spin dependent transport equations in drift-diffusion approximation and the detection of the spin current is through magneto-resistance. We discuss the various aspects of the ferromagnetic contacts, the insulating layer, and the spin relaxation inside the organic semiconductor on spin injection and its effects on magneto-resistance.

1.3 Organization of the thesis

This thesis is structured in five chapters. Each of chapters 2 to 4 consists of an introduction followed by model description, numerical results and discussion, and finally conclusions. The introduction deals with the relevant literature and the motivation of the work. The text of the thesis is organized in the following way:

In chapter 2 we describe spin injection from FM contacts into organic semiconductors. We discuss spin injection into organic semiconductors if the carrier injection mechanism is dominated by thermionic emission and by tunnelling.

Chapter 3 explains spin injection, transport of the spin through organic semiconductors, and detection of the resultant spin in organic spin valves. The tunnel layer is modeled as an ohmic layer with spin dependent contact resistances. We explore the various degrees of spin relaxation in the organic semiconductor on the detection of spin.

Spin polarized charge carrier injection and extraction by tunnelling through an insulating layer are modeled in chapter 4. A detailed description to calculate the

tunnelling time constants for spin up and spin down electrons is provided. We then model organic spin valve devices using these time constants and discuss the MR of organic spin valves.

Finally, chapter 5 presents the summary of the work and possible future directions. The thesis is wrapped up by Appendix A, where the solution of the spin diffusion equation is given.

Chapter 2

Spin Injection into organic semiconductors

The most essential requirement for a semiconductor based spintronic technology is the efficient electrical injection of spin polarized charge carriers from a FM contact into a semiconductor. In this chapter, we will explore that process. We consider a FM metal/semiconductor/non-magnetic metal device structure and will discuss the injection from the FM contact into the semiconductor. Initially, we will focus on the case of a FM metal in direct contact with the organic semiconductor. Later, we will consider the presence of a tunnel contact represented by spin dependent contact resistances.

2.1 Model parameters

In order to develop a model for carrier injection from FM contacts into organic semiconductors, we need to characterize the FM contact and the organic semiconductor by suitable parameters. The (non-magnetic) organic semiconductor is characterized by an energy gap, E_g, and by bands of conduction and valence states with narrow energy width. For the purpose of charge carrier population, these bands are described by equal effective densities of states, N_0, which are approximately equal to the molecular density of the material. (Neglecting the small spin-orbit coupling, equal effective densities of states $N_0/2$ may be attributed to spin up and spin down electrons and holes). The material is assumed to be undoped, hence all mobile charge carriers are injected from the contacts, and the large effective density of states ensures that non-degenerate statistics apply to essentially all cases of interest. The charge carrier mobility is independent of spin. It may be taken as field independent (as is reasonable for some organic molecular crystals) or it may be taken to be field dependent of the Poole-Frenkel form, $\mu(F)$ =

$\mu_0 \exp(|F|/F_0)^{1/2}$, where F is the electric field and μ_0 and F_0 are material parameters. For convenience we will assume field independent mobility and formulate the problem in terms of electron injection. In most cases, carrier injection into organic semiconductors is in fact due to holes. The spin physics of electrons and holes are essentially the same in organic semiconductors. Hence, modeling electron injection instead of hole injection does not affect the results and conclusion reached. Spin relaxation inside the organic semiconductor is described by a time constant, τ_s.

The FM metal contacts are described by four parameters: the total conductivity, σ, a polarization coefficient, α, the spin diffusion length, Λ, and the equilibrium Schottky barrier height, Φ_{B0}. The conductivities of spin up and spin down electrons are related to σ and α, as $\sigma_\uparrow = \alpha\,\sigma$ and $\sigma_\downarrow = (1-\alpha)\sigma$.

2.2 Spin and charge currents inside FM contacts

The current densities for the spin up (SU) and spin down (SD) electrons in the FM contacts can be written as:

$$j_\uparrow = \frac{\sigma_\uparrow}{e}\frac{d\mu_\uparrow}{dx} \tag{2.1a}$$

$$j_\uparrow = \frac{\sigma_\uparrow}{e}\frac{d\mu_\uparrow}{dx} \tag{2.1b}$$

where $\mu_{\uparrow,\downarrow}$ are the electrochemical potentials (or quasi-Fermi levels) for the SU and SD electrons, and e is the magnitude of the electron charge. Evidently, the charge current density is given by $j = j_\uparrow + j_\downarrow$, and the spin current density by $j_s = j_\uparrow - j_\downarrow$. Inside the bulk of the FM contact, the SU and SD electrons are in a quasi-equilibrium state, $\mu_\uparrow = \mu_\downarrow$, and the difference of the conductivities of SU and SD electrons give rise to a net spin current, $(2\alpha\text{-}1)\,j$. Under steady state conditions, the charge current is constant

throughout the entire structure. The spin current tends to decrease towards the interface to the non-magnetic semiconductor and the electrochemical potentials split. This is described by[52]

$$\frac{d^2(\mu_\uparrow - \mu_\downarrow)}{dx^2} = \frac{\mu_\uparrow - \mu_\downarrow}{\Lambda^2} \tag{2.2}$$

The splitting of the electrochemical potentials results in an increase in the ratio of the majority spin electron density to the minority spin electron density near the interface, which means that the majority and minority spin electrons are out of quasi-equilibrium near the interface of the FM contact and the semiconductor. We define the splitting between the electrochemical potentials as $\Delta\mu = \mu_\uparrow - \mu_\downarrow$. It can be easily derived from equations (2.1) and (2.2) that the spin current at the injecting contact interface ($x = 0^-$ as shown in figure 2.1) is

$$j_s(0^-) = (2\alpha - 1)j + 2\alpha(1-\alpha)\frac{\sigma}{\Lambda}\frac{\Delta\mu(0^-)}{e} \tag{2.3}$$

Since the current is negative, the magnitude of the spin current decreases by an amount of $2\alpha(1-\alpha)\sigma\Delta\mu(0^-)/e\Lambda$ at the interface relative to its bulk value of $(2\alpha\text{-}1)\,j$.

2.3 Transport in the organic semiconductor

Once the carriers are injected from the FM contact into the organic semiconductor, their transport is governed by the time and spin dependent continuity equations coupled with Poisson's equation.

$$\frac{\partial n_\uparrow}{\partial t} = \frac{\partial}{\partial x}\left(\mu n_\uparrow F + D\frac{\partial n_\uparrow}{\partial x} \right) - \frac{n_\uparrow - n_\downarrow}{\tau_s}, \tag{2.4a}$$

$$\frac{\partial n_\downarrow}{\partial t} = \frac{\partial}{\partial x}\left(\mu n_\downarrow F + D\frac{\partial n_\downarrow}{\partial x} \right) - \frac{n_\downarrow - n_\uparrow}{\tau_s}, \tag{2.4b}$$

$$\frac{\partial F}{\partial x} = -\frac{4\pi e}{\varepsilon}(n_\uparrow + n_\downarrow). \tag{2.5}$$

Here $n_\uparrow$ and $n_\downarrow$ are the SU and SD electron concentrations and D is the electron diffusivity which is related to the mobility, μ, through the Einstein relation, and ε is the static dielectric constant. Evidently the charge ($n = n_\uparrow + n_\downarrow$) and spin ($n_s = n_\uparrow - n_\downarrow$) continuity equations become simply,

$$\frac{\partial n}{\partial t} = \frac{\partial}{\partial x}\left(\mu n F + D\frac{\partial n}{\partial x} \right) \tag{2.6}$$

$$\frac{\partial n_s}{\partial t} = \frac{\partial}{\partial x}\left(\mu n_s F + D\frac{\partial n_s}{\partial x} \right) - \frac{2n_s}{\tau_s} \tag{2.7}$$

Equations (2.4) and (2.5) can be solved numerically specifying the boundary conditions. We discretize these equations spatially using the Scharfetter-Gummel approach[53] and the resulting first order differential equations are integrated forward in time. To find the steady state solution at an applied voltage bias, a time dependent potential ramp that stops at the desired voltage is applied to the right contact and the equations are integrated forward in time starting from the thermal equilibrium until steady state is reached. The

position independence of the charge current is used to verify that steady state has been reached. The equilibrium state is calculated following the approach described in ref. 33.

The boundary conditions are given by specifying the currents for each spin type at the boundary. The currents at the boundary depend on the injection/extraction mechanism between the contacts and the semiconductor. We will consider two kinds of injection mechanisms. First, we will consider current injection by thermionic emission over the Schottky barrier that the semiconductor forms with the contact metal. In this case, the metal is in direct contact with the semiconductor. Second, we will consider current injection by tunnelling into organic semiconductors. In this case the metal contact is separated from the semiconductor by a thin insulating layer.

2.4 Injection by thermionic emission

A schematic energy level diagram of the injecting contact for thermionic emission is shown in figure 2.1 under bias conditions. Also shown is the image-charge induced barrier lowering effect. In this model, the injected current for each spin direction, $j_{inj;\uparrow,\downarrow}$ is the sum of a thermionic emission current and an interface recombination current (which is the time reverse process of thermionic emission). The spin dependent currents at the semiconductor interface ($x = 0^+$ as shown in figure 2.1) are given by[54]

$$j_{inj;\uparrow}(0^+) = A^* T^2 \left[\frac{n_\uparrow(0^+)}{N_0} - \frac{1}{2} \exp\left(-\Phi_{B;\uparrow} / kT\right) \right] \tag{2.8a}$$

$$j_{inj;\downarrow}(0^+) = A^* T^2 \left[\frac{n_\downarrow(0^+)}{N_0} - \frac{1}{2} \exp\left(-\Phi_{B;\downarrow} / kT\right) \right] \tag{2.8b}$$

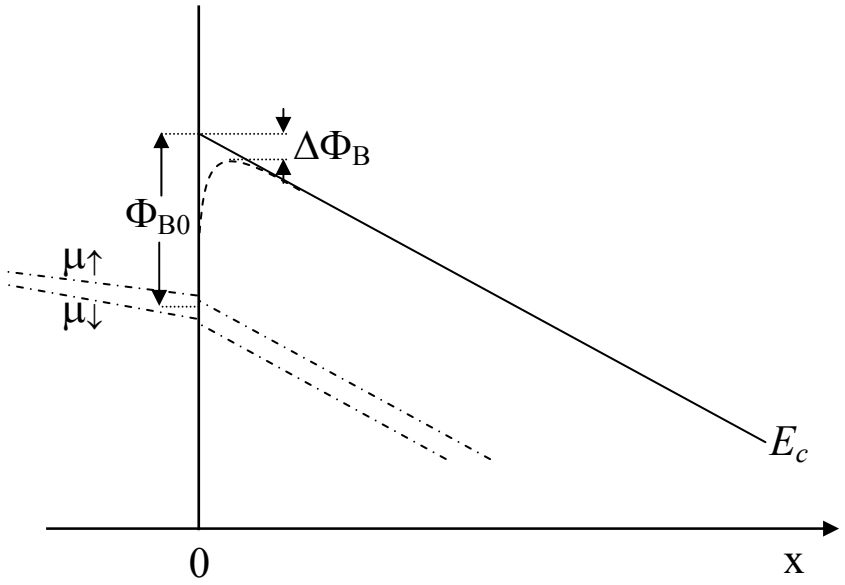

Figure 2.1. Schematic energy band diagram of a Schottky contact between a FM metal and a semiconductor under bias such as to enable injection of electrons into the semiconductor.

Here A^* denotes the effective Richardson constant, T the temperature, k Boltzmann's constant, and $\Phi_{B;\uparrow,\downarrow}$ the spin dependent non-equilibrium barrier height. The barrier height depends on spin because the quasi-Fermi levels are different for the two spin directions as shown in figure 2.1. The spin dependent electron concentrations in the semiconductor at the interface are denoted by $n_{\uparrow,\downarrow}(0^+)$. Image charge induced Schottky barrier lowering is comparatively strong in the organic semiconductors due to their small dielectric constants. The effect may be approximated by lowering the equilibrium barrier height by: $\Delta\Phi_B \propto \sqrt{eF(0^+)/\varepsilon}$, where $F(0^+)$ is the electric field in the semiconductor. Image charge induced barrier lowering is included in the determination of the value of $\Phi_{B;\uparrow,\downarrow}$. The Schottky barrier, Φ_B, and spin dependent barriers $\Phi_{B;\uparrow,\downarrow}$ are related to the spin

dependent electrochemical potentials at the contact and the conduction band edge, E_c, through

$$\Phi_B = E_c(0^+) - \frac{\mu_\uparrow(0^+) + \mu_\downarrow(0^+)}{2} \tag{2.9a}$$

$$\Phi_{B;\uparrow} = E_c(0^+) - \mu_\uparrow(0^+), \tag{2.9b}$$

$$\Phi_{B;\downarrow} = E_c(0^+) - \mu_\downarrow(0^+), \tag{2.9c}$$

The injected charge current density, j_{inj}, is the sum of the SU and SD currents given by equations (2.8a) and (2.8b), which can be combined to:

$$j_{inj}(0^+) = AT^2\left[\frac{n(0^+)}{N_0} - \exp\left(-\frac{\Phi_B}{kT}\right)\cosh\left(\frac{\Delta\mu(0^+)}{2kT}\right)\right] \tag{2.10}$$

Here $n(0^+)$ is the total ($n_\uparrow + n_\downarrow$) electron concentration in the semiconductor at the interface. Similarly the injected spin current density, $j_{s,inj} = j_{inj;\uparrow} - j_{inj;\downarrow}$, can be expressed as

$$j_{s,inj}(0^+) = AT^2\left[\frac{n_s(0^+)}{N_0} - \exp\left(-\frac{\Phi_B}{kT}\right)\sinh\left(\frac{\Delta\mu(0^+)}{2kT}\right)\right], \tag{2.11}$$

where $n_s(0^+)$ is the electron spin ($n_\uparrow - n_\downarrow$) concentration at the interface. The key part of this model is to determine the splitting between the electrochemical potentials at the contact i.e. $\Delta\mu(0^+)$. We assume that there is no spin scattering as the electrons traverse the FM/semiconductor interface. Hence, both the spin current and the charge current are

continuous across the interface and the splitting of the quasi-Fermi levels at both sides of the interface is the same:

$$j(0^-) = j_{inj}(0^+) = j, \tag{2.12a}$$

$$j_s(0^-) = j_{s,inj}(0^+) = j_s(0). \tag{2.12b}$$

$$\Delta\mu(0^-) = \Delta\mu(0^+) = \Delta\mu(0) \tag{2.12c}$$

Equations (2.3), (2.9a)-(2.9c), (2.10), (2.11), and (2.12a)-(2.12c) are used to determine the spin dependent barrier heights $\Phi_{B;\uparrow,\downarrow}$, which are used to determine the spin dependent particle currents at the boundary (equations (2.8a) and (2.8b)).

The splitting between the electrochemical potentials $\Delta\mu(0)$ is small due to the high conductivity of the FM metal, and if $\Delta\mu(0)<<2kT$, the electron spin density, the charge current, and the spin current at the injecting contact can be approximated by:

$$n_s(0^+) = n(0^+)\frac{\Delta\mu(0)}{2kT}, \tag{2.13a}$$

$$j = AT^2\left[\frac{n(0^+)}{N_0} - \exp\left(-\frac{\Phi_B}{kT}\right)\right], \tag{2.13b}$$

$$j_s(0) = AT^2\left[\frac{n_s(0^+)}{N_0} - \exp\left(-\frac{\Phi_B}{kT}\right)\frac{\Delta\mu(0)}{2kT}\right], \tag{2.13c}$$

We can eliminate the electrochemical potentials from equations (2.3) and (2.13) and express the spin current as a function of the charge current:

$$j_s(0) = \frac{-(2\alpha - 1) j^2}{2\alpha(1-\alpha)\frac{\sigma}{\Lambda}\frac{2kT}{e} - j} \tag{2.14}$$

For electron injection we have $j < 0$. Equation (2.14) is valid provided that the current injection is dominated by thermionic emission and its time reverse, interface recombination. From equation (2.14), we can draw two conclusions. First, when α tends to one, the spin current approaches the charge current. Second, if the ratio σ/Λ for the contact material is sufficiently small, the spin current is equal to $(2\alpha\text{-}1)j$, which is the spin current in the bulk of the FM contact. Hence, in order to achieve significant spin injection we need either strongly polarized contacts $(\alpha \approx 1)$ or a contact material that has small σ/Λ. For conventional FM metal contacts, where the spin polarization is not close to one and the σ/Λ ratio is large, equation (2.14), can be further approximated by

$$\frac{j_s(0)}{j} = \frac{-(2\alpha - 1) j}{2\alpha(1-\alpha)\frac{\sigma}{\Lambda}\frac{2kT}{e}} \tag{2.15}$$

Here $j_s(0)/j$ is the spin polarization, SP, of the injected current.

2.5 Numerical results for thermionic emission

We considered an organic semiconductor, 100 nm thick, sandwiched between a FM contact and a non-magnetic metal contact. The FM contact forms a Schottky barrier of 0.3 eV with the semiconductor. A contact made from colossal magneto-resistance manganates, LSMO, is also considered. LSMO acts nearly as half metal, where $\alpha \rightarrow 1$. The transport parameters adopted for a FM metal, LSMO, and the organic semiconductor are listed in table 2.1.

Table 2.1 Transport parameters

	σ (S/cm)	α	Λ (cm)
FM metal	10^5	0.9	10^{-5}
CMR half-metal	10	≈ 1	10^{-6}
Organic Semiconductor	E_g (eV)	μ (cm^2/Vs)	N_0 (cm^{-3})
	2.4	10^{-2}	10^{21}

First, we consider spin injection from a FM metal contact into an organic semiconductor. Figure 2.2 shows the calculated injected charge and spin current densities as a function of the voltage applied. The charge current density is constant throughout the structure as required by charge conservation, but the spin current density varies due to spin relaxation. The spin current density shown in figure 2.2 is evaluated at

the electron injecting contact. The spin current density is much smaller than the charge current density due to the high electrical conductivity and short spin diffusion length of the contact metal. The dotted line shows the approximate spin current density obtained from the charge current density via Eq. (2.15). The dotted line essentially coincides with the dashed line (numerically calculated result), indicating that the spin current is to a good approximation proportional to the square of the charge current. This parabolic dependence of spin current on charge current can be explained by the large conductivity mismatch between the metallic contact and the organic semiconductor.

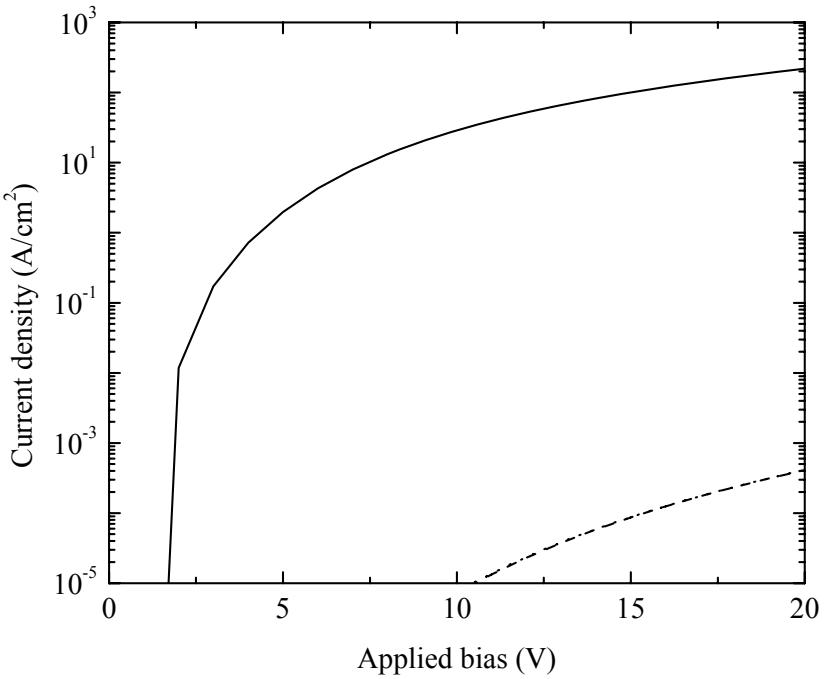

Figure 2.2. Calculated charge (solid), calculated spin (dashed), and approximate spin (dotted – Eq. 2.15) current densities as a function of the applied voltage across the device structure with a FM metal injecting contact.

At low bias, charge carrier injection is low, implying that the conductivity of the semiconductor is low. As the bias voltage increases, the charge carrier injection increases, which increases the semiconductor conductivity and reduces the conductivity mismatch between the semiconductor and the FM metal, and spin current increases with the charge current.

Next, we consider spin injection from LSMO. Figure 2.3 displays the calculated injected charge and spin current densities from LSMO contacts into an organic semiconductor for different contact polarizations, α. Again the spin current density shown in figure 2.3 is taken at the electron injecting contact. Evidently, spin injection is greatly enhanced only when the contact is nearly half-metallic. Two parameters assist high spin injection. One is a low conductivity of the contact, which for half-metals like LSMO is almost four orders magnitude smaller than that of conventional FM metals. The other is the high contact polarization of the half-metallic contact, which is close to unity. From figure 2.3, we can see that, as we increase α, the spin current increases and tends towards the charge current. It is also evident that α needs to approach unity very closely in order to be effective in enabling strong spin injection.

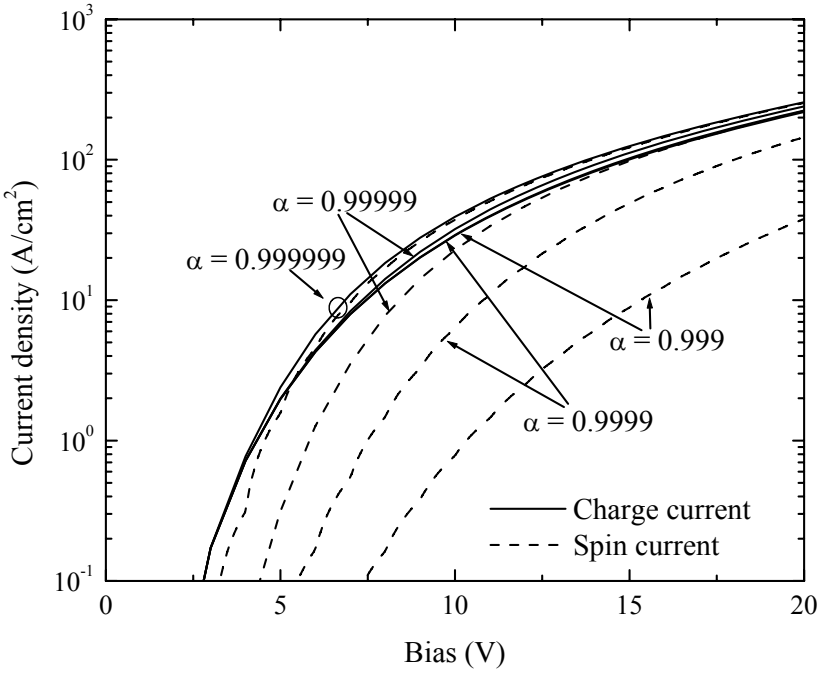

Figure 2.3. Calculated charge (solid) and spin (dashed) current densities as a function of the applied voltage across the device structure with LSMO as the injecting contact. Contact polarization, α is used as a parameter.

We next explore how the spin current predicted by equation (2.14) matches with the calculated spin current for LSMO injecting contact. We plot the numerically calculated spin current and eq. (2.14) as a function of the injected charge current in figure 2.4. The simple analytical results (dotted lines) nicely match the calculated spin currents (dashed lines) for all values of α. This result indicates that the analytical expression given by Eq. (2.14) is a good approximation of the injected spin current for any FM contacts provided that the current injection is dominated by thermionic emission.

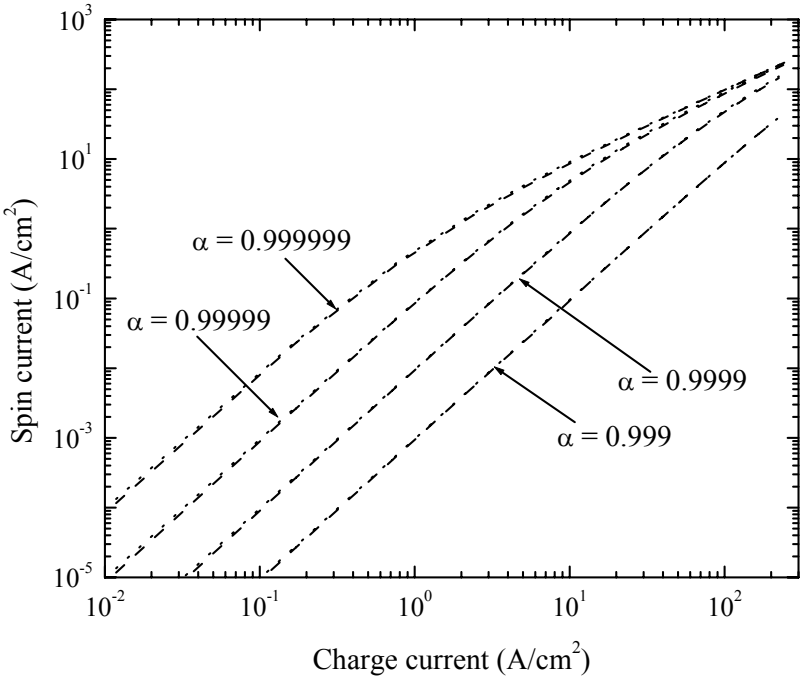

Figure 2.4. Numerically calculated spin current (dashed) and analytical spin current (dotted) projected from the charge current (Eq. 2.14) as a function of the injected charge current for LSMO injecting contact. Contact polarization, α is used as a parameter.

2.6 Injection by tunnelling

To model injection by tunnelling, we may envision a thin insulating tunnel layer between the FM contact and the semiconductor as shown in figure 2.5. Electron tunnelling from a FM contact through this layer is spin selective because the spatial part of electron wave function is different for majority and minority spin direction. The

tunnelling process through the insulating layer can be described by spin dependent contact resistances, $r_\uparrow$ and $r_\downarrow$, for the SU and SD electrons respectively. We assume that the tunnel layer is more transparent for the majority spin electrons such that $r_\uparrow < r_\downarrow$.

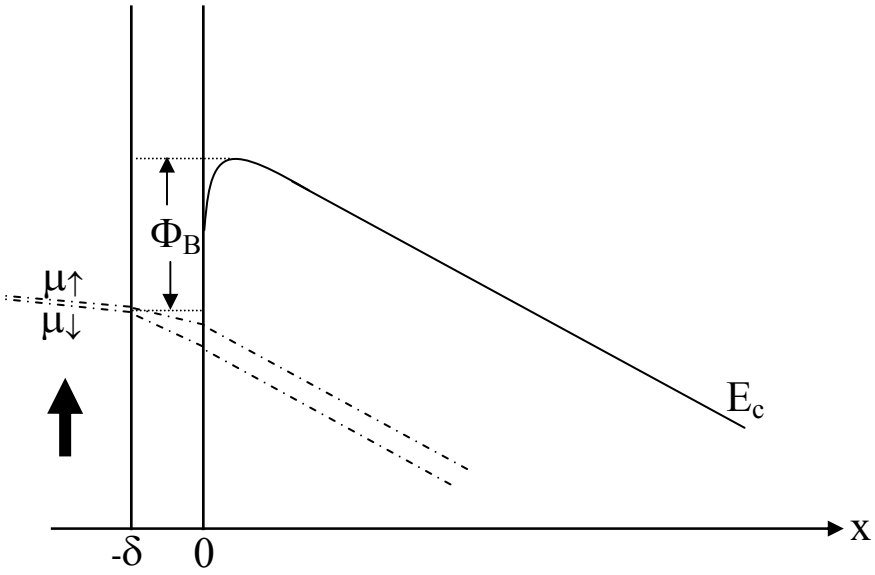

Figure 2.5. Schematic energy band diagram for a contact between a ferromagnetic metal and a semiconductor through a thin insulating tunnel layer under bias.

If there is no spin scattering in the insulating layer, the current for each spin direction is continuous and is related to the spin dependent electrochemical potential change across the tunnel layer via Ohm's law, giving rise to the following boundary conditions:

$$\mu_\uparrow(0) - \mu_\uparrow(-\delta) = r_\uparrow j_\uparrow(-\delta) \tag{2.16a}$$

$$\mu_\downarrow(0) - \mu_\downarrow(-\delta) = r_\downarrow j_\downarrow(-\delta) \tag{2.16b}$$

$$j_s(-\delta) = j_s(0) \tag{2.16c}$$

Equations 2.16(a)-(c) can be used to calculate the difference of the quasi-Fermi levels at the insulator/semiconductor interface, and it is given by:

$$\Delta\mu(0) = \Delta\mu(-\delta) + \frac{1}{2}e\left(r_\uparrow - r_\downarrow\right)j + \frac{1}{2}e\left(r_\uparrow + r_\downarrow\right)j_s(0) \tag{2.17}$$

Here we allow for a possible additional discontinuity $\Delta\mu(-\delta)$ in the quasi-Fermi levels at the contact/insulator interface as it occurs for example if carrier injection is limited by thermionic emission in the absence of the tunnel barrier. It is convenient to combine the effects of the FM metal and the tunnel contact and to express the polarization effect in the semiconductor in terms of $\Delta\mu(0)$

$$\Delta\mu(0) = \frac{1}{2}e\left(r'_\uparrow - r'_\downarrow\right)j + \frac{1}{2}e\left(r'_\uparrow + r'_\downarrow\right)j_s(0) \tag{2.18}$$

where the effective resistances are defined by:

$$r'_\uparrow - r'_\downarrow = r_\uparrow - r_\downarrow - \frac{(2\alpha - 1)\Lambda}{\alpha(1-\alpha)\sigma} \approx r_\uparrow - r_\downarrow \tag{2.19a}$$

$$r'_\uparrow + r'_\downarrow = r_\uparrow + r_\downarrow + \frac{\Lambda}{\alpha(1-\alpha)\sigma} \approx r_\uparrow + r_\downarrow \tag{2.19b}$$

because Λ/σ tends to be very small for conventional ferromagnetic metals on the scale of the contact resistances. Once the difference of the quasi-Fermi levels are defined in the

form of equation (2.18), we can calculate the injected charge and spin currents using the model developed in section 2.4, i.e. by using equations (2.9)-(2.12).

2.7 Numerical results for tunnel injection

The spin current and the charge current in the presence of spin dependent contact resistances are plotted in figure 2.6. The device parameters are the same as discussed in the case of thermionic emission. The values of the spin selective contact resistances are: $r_{\uparrow} = 5\times10^{-3}\ \Omega\ cm^2$ and $r_{\downarrow} = 10^{-2}\ \Omega\ cm^2$, such that $r_{\uparrow}/\ r_{\downarrow} = 1/2$. In the plot, we exclude the voltage drop across the contact resistance, as it is negligible compared to the overall applied bias. At thermal equilibrium, electron spins are polarized in the FM contact but unpolarized in the semiconductor. In the absence of contact resistances, the electrons in the metal and in the semiconductor are in good thermal contact, and therefore the electrons in the semiconductor stay close to local thermal equilibrium. In order to achieve effective spin injection, this quasi-equilibration must be suppressed. The spin dependent contact resistance breaks the quasi-equilibration between the organic semiconductor and the metallic contact and greatly enhances spin injection from the metallic contact into the semiconductor as evident in figure 2.6.

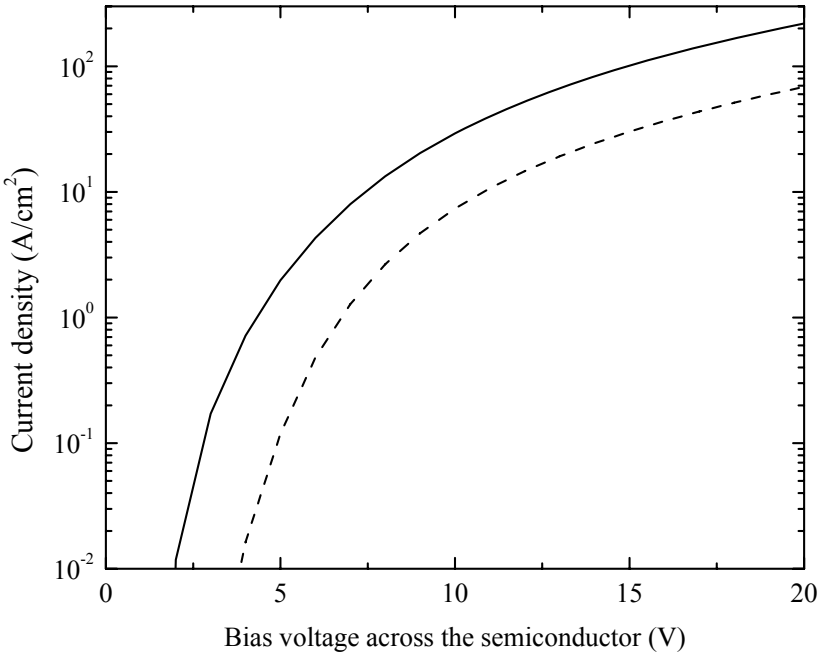

Figure 2.6. Injected charge (solid) and spin (dashed) current densities from a FM metal contact into the organic semiconductor in the presence of spin selective contact resistances. The values of the contact resistances are $r_{\uparrow} = 5\times10^{-3}$ Ω cm^2 and $r_{\downarrow} = 10^{-2}$ Ω cm^2.

Next we explore how the magnitude and the ratio of the spin dependent contact resistances affect spin injection. We can control the spin polarization, $j_s(0)/j$, of the injected current by controlling the spin dependent contact resistances, $r_{\uparrow}$ and $r_{\downarrow}$. At a given level of charge injection, spin injection can be increased either by increasing the contact resistances (while keeping the ratio $r_{\uparrow}/ r_{\downarrow}$ constant) or by decreasing the ratio $r_{\uparrow}/ r_{\downarrow}$ (while keeping $r_{\uparrow}$ constant). Figure 2.7 shows the relative SP for different combinations of contact resistances. Again, the bias voltage is taken only across the

organic semiconductor in order to indicate a given level of charge injection. Charge injection is the same in all cases at a given bias across the semiconductor. From figure 2.7, we can conclude that spin injection can be increased either by increasing the contact resistances (while keeping $r_\uparrow / r_\downarrow$ constant) or by decreasing the ratio of $r_\uparrow / r_\downarrow$ (while keeping $r_\uparrow$ constant). Decreasing the ratio of $r_\uparrow / r_\downarrow$ has a more pronounced effect on SP over increasing the magnitude of the resistances. Moreover, increasing the contact resistances increases the voltage drop across the contacts. For a fixed ratio $r_\uparrow / r_\downarrow$, increasing the contact resistances increases the spin polarization significantly when the bias voltage is low. For large biases, increasing the contact resistances with fixed $r_\uparrow / r_\downarrow$ ratio has negligible effect on spin polarization.

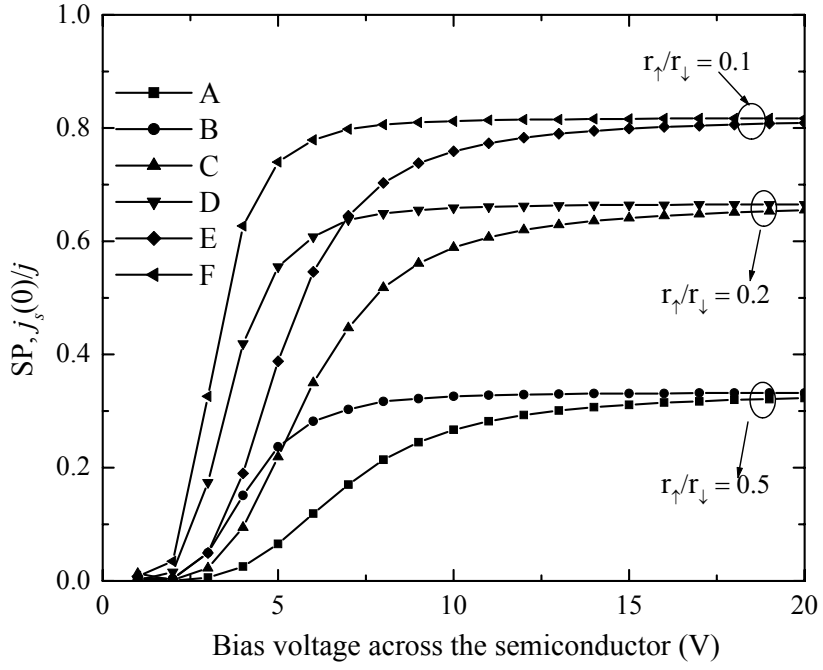

Figure 2.7. SP, $j_s(0)/j$, for different combinations of spin selective contact resistances. The values of the contact resistances are give in table 2.2.

Table 2.2. Spin selective contact resistances for the different plots shown in figure 2.7

Plot	$r_\uparrow$ (Ω cm^2)	$r_\downarrow$ (Ω cm^2)	$r_\uparrow / r_\downarrow$
A	5×10^{-3}	10^{-2}	0.5
B	5×10^{-2}	10^{-1}	0.5
C	5×10^{-3}	2.5×10^{-2}	0.2
D	5×10^{-2}	2.5×10^{-1}	0.2
E	5×10^{-3}	5×10^{-2}	0.1
F	5×10^{-2}	5×10^{-1}	0.1

2.8 Conclusions

We may summarize these results as follows: thermionic emission cannot inject spin polarized charge carriers from a conventional ferromagnetic metal contact into organic semiconductors, and effects such as image charge induced barrier lowering do not alter that conclusion. The physical reason for inefficient spin injection is as follows. At thermal equilibrium, the FM contact is spin polarized but the semiconductor is unpolarized. For a FM metal/semiconductor junction, the electrons in the metal and in the semiconductor are in good contact, and therefore the electrons in the semiconductor stay close to local thermal equilibrium. As a result, the charge carriers in the semiconductor are only weakly spin polarized, but spin polarization increases slowly with

increasing bias, i.e. when the semiconductor is driven further out of equilibrium. In order to drive the semiconductor far out of equilibrium, we need to inject a high charge current density; within practical values for the injected charge current density, the spin current density remains orders magnitude smaller than the charge current density. On the other hand an LSMO contact may enhance spin injection. However, spin injection from the LSMO contact is appreciable only if the contact is indeed very close to half metallic. In other words spin polarization of the contact should be 99.999%, which is practically impossible at a reasonable temperature.

Spin injection is greatly enhanced if there is a spin dependent contact resistance between the metallic contact and the semiconductor. An insulating tunnel barrier with a spin polarized FM contact has spin dependent interface resistance because of the difference in Fermi wave vectors for the two spin types in the contact material. A FM insulator tunnel barrier can also provide spin dependent contact resistance.[55] The spin dependent contact resistance breaks the quasi-equilibration between the organic semiconductor and the FM contact and significantly enhances spin injection.

Chapter 3

Spin transport and its detection in organic spin valves

A theory of spin injection was developed in the previous chapter. We showed that a spin dependent contact resistance (tunnel barriers) at the injecting contact can greatly enhance spin injection. The resulting spin polarization is, in principle, detectable through the extracting contact via the MR of a spin valve. In this chapter we will explore spin transport through the organic semiconductor and detection of the spin polarization.

3.1 Device structures

The device structures we will consider in this chapter consist of an organic semiconductor of thickness L sandwiched between two FM contacts – a device commonly known as an organic spin valve. Fig 2.1 shows such a schematic device structure. In this spin valve geometry envisioned, the left electrode is the injecting contact and right electrode is the extracting contact. The polarization of the left electrode is always in the up-direction. For parallel alignment of contact magnetization, the polarization of the right electrode is in the up-direction, whereas for anti-parallel alignment, the polarization of the right electrode is in the down-direction. The spin

dependent contact resistances are such that for spin up polarization of the contact, $r_{\uparrow} < r_{\downarrow}$, and vice versa.

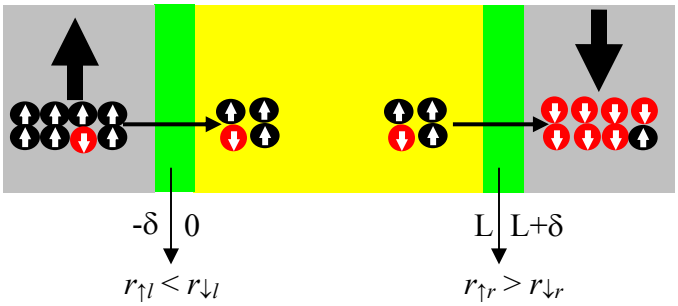

Figure 3.1. A schematic device structure consisting of an organic semiconductor sandwiched between two FM contacts with anti-parallel contact magnetizations. The effects of the tunnel barriers are described by spin dependent contact resistances.

3.2 Splitting of quasi-Fermi levels at the contacts

The spin dependent contact resistances increase the splitting between the quasi-Fermi levels at the semiconductor/tunnel barrier interface as discussed in section 2.6. The splitting at the injecting and extracting contacts are given by[56]

$$\Delta\mu(0) = \frac{1}{2}e\left(r_{\uparrow l} - r_{\downarrow l}\right)j + \frac{1}{2}e\left(r_{\uparrow l} + r_{\downarrow l}\right)j_s(0) \tag{3.1a}$$

$$\Delta\mu(L) = \frac{1}{2}e\left(r_{\uparrow r} - r_{\downarrow r}\right)j + \frac{1}{2}e\left(r_{\uparrow r} + r_{\downarrow r}\right)j_s(L) \tag{3.1b}$$

Here *l* and *r* identify the left and right contacts, respectively.

3.3 Transport in the semiconductor

Under steady state conditions, the carrier transport in the organic semiconductor is governed by the spin dependent continuity equations,

$$\mu \frac{d}{dx}\left(n_{\uparrow} F + \frac{kT}{e}\frac{dn_{\uparrow}}{dx} \right) - \frac{n_{\uparrow} - n_{\downarrow}}{\tau_s} = 0, \tag{3.2a}$$

$$\mu \frac{d}{dx}\left(n_{\downarrow} F + \frac{kT}{e}\frac{dn_{\downarrow}}{dx} \right) - \frac{n_{\downarrow} - n_{\uparrow}}{\tau_s} = 0, \tag{3.2b}$$

where the SU and SD currents are expressed in drift-diffusion approximation. Here $n_{\uparrow,\downarrow}$ are the spin dependent electron densities, F is the electric field, k is Boltzmann's constant, and T is the temperature. The carrier mobility and spin relaxation time are denoted by μ and τ_s, respectively. Non-degenerate carrier statistics is assumed for the organic semiconductor. The continuity equations are to be solved together with Poisson's equation,

$$\frac{dF}{dx} = -4\pi e(n_{\uparrow} + n_{\downarrow})/\varepsilon \tag{3.3}$$

where ε is the permittivity of the semiconductor.

It is instructive first to consider a case in which an essentially analytical solution to the transport problem may be obtained. We make the following approximations: (i) τ_s

is long compared to the transit time, i.e. the last terms in equations (3.2a) and (3.2b) are neglected; (ii) the effect of the injected space charge is neglected, i.e. the electric field is constant throughout the organic semiconductor; and (iii) ohmic boundary conditions apply, i.e. $\mu_{\uparrow}$ and $\mu_{\downarrow}$ are continuous at $x = 0$ and $x = L$. The resulting charge current and spin current in the organic semiconductor can then be expressed as,

$$j = F(V')\left[\exp\left(\frac{V'}{kT}\right)\times\cosh\left(\frac{\Delta\mu(0)}{2kT}\right)-\cosh\left(\frac{\Delta\mu(L)}{2kT}\right)\right] \tag{3.4a}$$

$$j_s = F(V')\left[\exp\left(\frac{V'}{kT}\right)\times\sinh\left(\frac{\Delta\mu(0)}{2kT}\right)-\sinh\left(\frac{\Delta\mu(L)}{2kT}\right)\right] \tag{3.4b}$$

V' is the voltage dropped across the semiconductor, and $F(V')$ is given by,

$$F(V') = \frac{-e\mu\dfrac{V'-V_b}{L}N_0\exp\left(-\dfrac{\Phi_{B;r}}{kT}\right)}{\exp\left(\dfrac{V'-V_b}{kT}\right)-1} \tag{3.5}$$

Here V_b is the built-in potential, ($\Phi_{B;r}$ - $\Phi_{B;l}$) and $\Phi_{B;r(l)}$ are the barrier heights of the right (left) contact. We assume $\tau_s >> L^2/(\mu kT/e)$, hence the injected spin current density is constant throughout the semiconductor. From Eqs. (3.4a) and (3.4b), we see that if $V' >> kT$, the charge and spin currents depend only on the difference of the quasi-Fermi levels at the left (injecting) electrode. However, in the low bias regime, both the injecting and extracting contacts control the currents in the semiconductor. Equations (3.1) and (3.4)

can be solved self-consistently for a particular bias, *V'*. The total voltage applied to the device is then obtained from,

$$V = V' + \Delta V_l + \Delta V_r \tag{3.6a}$$

$$\Delta V_{l,r} = -(1/4)[(r_{\uparrow l,r} + r_{\downarrow l,r})j + (r_{\uparrow l,r} - r_{\downarrow l,r})j_s] \tag{3.6b}$$

Spin dependent contact resistances greatly enhance spin injection and the resulting spin polarization can be extracted via the MR of the organic spin valve. The MR is defined as the difference of the resistances between anti-parallel (AP) and parallel (P) alignments of the contact magnetizations. The P and AP configurations are expressed through the terms involving $r_{\uparrow r} - r_{\downarrow r}$, which have the same sign as $r_{\uparrow l} - r_{\downarrow l}$ in P configuration, but opposite sign in AP configuration. Thus, the currents and total applied voltages for the two contact alignments are obtained as a function of *V'*. Finally, the MR is defined as,

$$\mathrm{MR} = \left(\frac{V_{AP}}{V_P} \frac{j_P}{j_{AP}} - 1 \right) \times 100\% \tag{3.7}$$

Here V_{AP} and V_{P} denote the applied biases for the P and AP configurations, and j_{P} and j_{AP} are the corresponding charge current densities.

3.4 Results without spin relaxation

We use the calculation outlined above for relatively thin organic semiconductor layers where space charge effects due to the injected carriers are small under low bias. The thickness L is taken to be 100nm, and the mobility is 10^{-2}cm^2/Vs. The spin relaxation time thus needs to be much greater than 400ns to be consistent with our approximations above. For simplicity, we take $V_b = 0$, and choose a barrier height of 0.2eV. All calculations are for room temperature conditions.

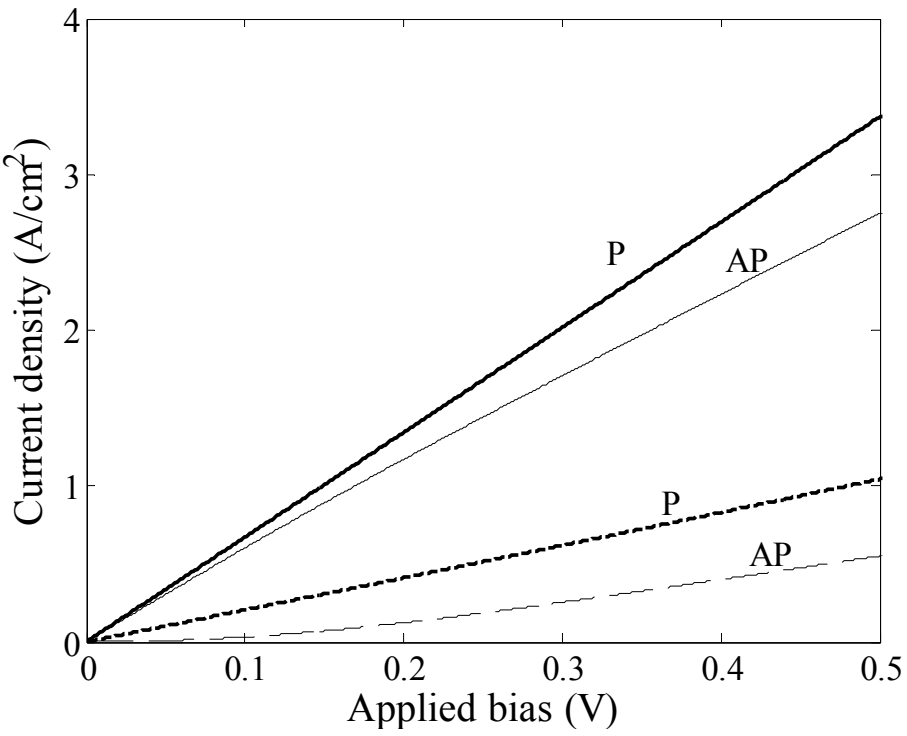

Figure 3.2. Charge current density (solid curves) and spin current density (dashed curves) for P and AP contact magnetizations as a function of applied bias. The ratios of $r_\uparrow / r_\downarrow$ for both left and right contacts are ½ and $r_{\uparrow l} = 10^{-1}\Omega cm^2 = r_{\uparrow r}$.

Figure 3.2 shows the calculated charge and spin currents versus total applied voltage for P and AP alignments. The ratios $r_{\uparrow} / r_{\downarrow}$ for both left and right contacts are ½ and $r_{\uparrow_l} = 10^{-1}\Omega cm^2 = r_{\uparrow_r}$. We also consider cases in which the contact resistance values of the injecting and extracting contacts are different. The current polarizations for three cases are depicted in figure 3.3.

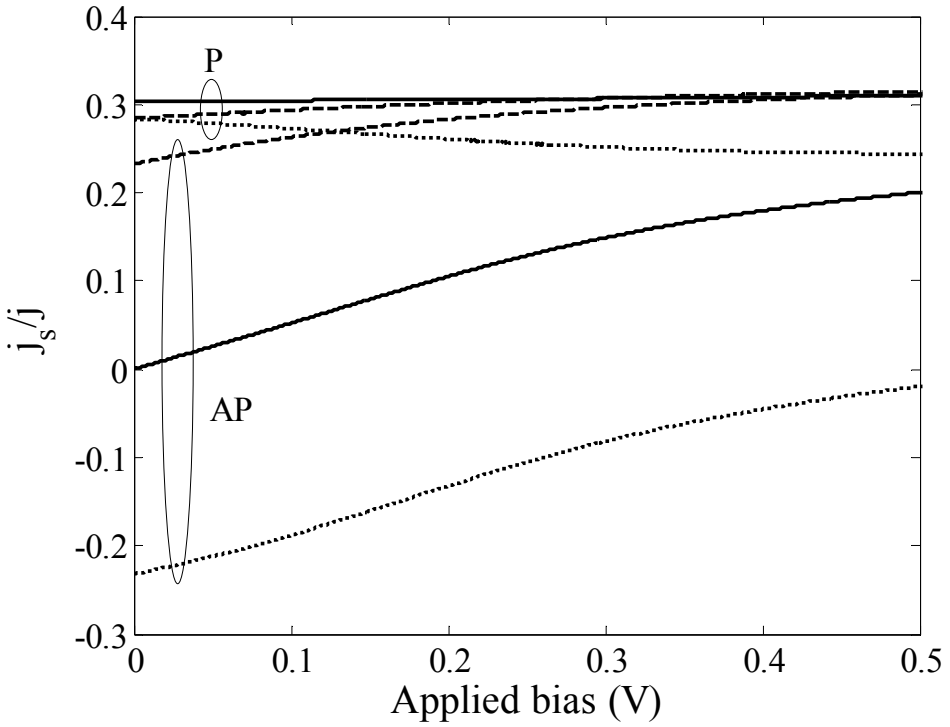

Figure 3.3. Spin polarization, j_s/j, for P and AP contact alignments and different effective contact resistances. The ratios of $r_{\uparrow} / r_{\downarrow}$ for both left and right contacts are ½ in all cases. The magnitudes of the contact resistances are $r_{\uparrow_l} = 10^{-1}\Omega cm^2 = r_{\uparrow_r}$ (solid lines), $r_{\uparrow_l} = 10^{-1}\Omega cm^2 = 10 r_{\uparrow_r}$ (dashed lines), and $10 r_{\uparrow_l} = 10^{-1}\Omega cm^2 = r_{\uparrow_r}$ (dotted lines).

Here the results for effective contact resistances are compared with those obtained for reduced effective resistances on the injecting or the collecting side. It can be seen that in the non-symmetric situations even in the AP alignment case the current polarization extrapolates to a non-zero value at vanishing bias. If the effective contact resistance of the extracting contact is larger than that of the injecting contact, it tends to determine the spin polarization at low bias, which in the sign convention adopted here is negative. Figure 3.4 shows the calculated MR values for three sets of effective contact resistances. It is evident that the MR may decrease with increasing bias if the effective contact resistances of the injecting contact are smaller than those of the extracting contact.

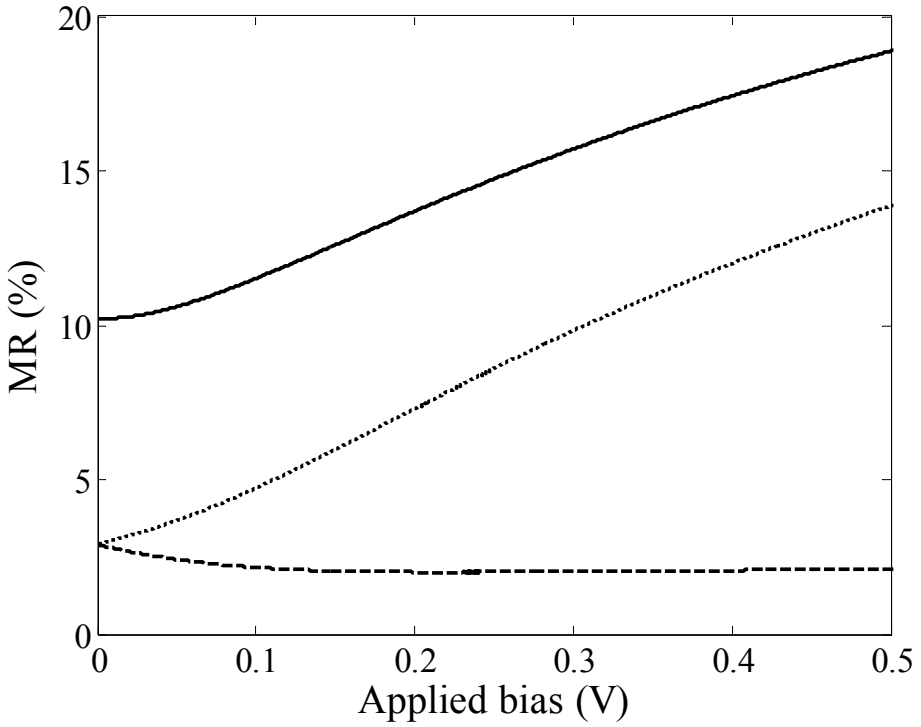

Figure 3.4. MR plotted as a function of the applied bias for three cases of different effective contact resistances as shown in figure 3.3.

The model calculations above yield magneto-resistances that increase or decrease moderately with increasing voltage at low bias and that increase monotonically with increasing voltage at high bias. As explained in Chapter 2 and also evident from figures 3.2 and 3.3, spin injection increases with increasing applied bias. For linear contact resistances, the increase in the spin injection increases the MR with increasing applied bias as evident from figure 3.4. However, essentially all successful experiments to date show decreasing MR with increasing bias. Thus far, we have treated the effective contact resistances as linear, i.e. independent of the bias. This may be appropriate for the part that originates directly from the transport parameters of the FM metal (see equation 2.19, page 24), but it is unlikely to be correct for the part attributed to spin selective tunnelling through an insulating interfacial layer. For the latter, which as argued above is likely to dominate $r_{\uparrow}$ and $r_{\downarrow}$, a relatively strong decrease with increasing bias is expected. A very simple heuristic model that accounts only for the population effects at energies relevant for injection (and above the metal Fermi level by approximately Φ_B) leads to a bias dependence of the contact resistance of form, $r_{\uparrow\downarrow}(\delta V) = r_{\uparrow\downarrow}(0)\exp(-\delta V / kT)$. Here $\delta V \approx \Delta V$ is the voltage dropped across the contact barrier layer. The exponential decrease of the contact resistances with increasing bias has also been suggested previously by A. Fert and H. Jaffrès. The actual bias dependence of the contact resistances is likely to be stronger, but, to explore the effect qualitatively, we insert this type of dependence for the injecting and extracting contact resistances into the analytical model and re-examine the low voltage range explored in figures 3.2 – 3.4. The resulting current polarization and MR are plotted in figures 3.5 and 3.6.

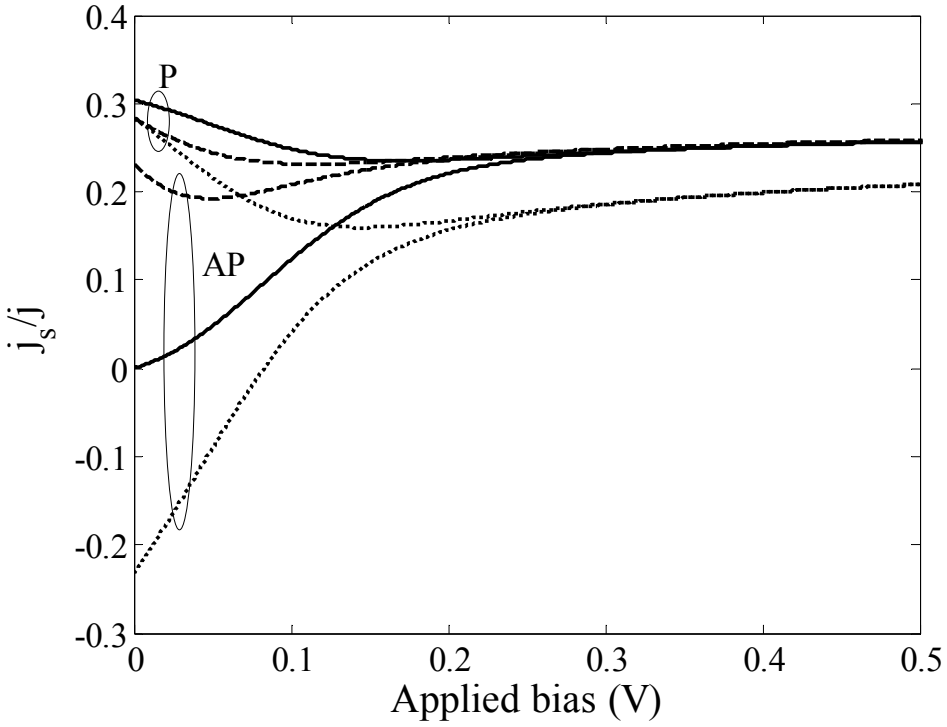

Figure 3.5. Spin polarization, j_s/j, for P and AP contact magnetizations for the three cases as shown in figure 3.3. Here the contact resistances are allowed to vary with bias across the layer as described in the text. The $\Delta V = 0$ values are the same as those in figure 3.3.

It is evident, that current polarizations decrease relative to the case of constant effective contact resistances, but most striking is the decrease of the MR with increasing bias. The magnitude of the contact resistances decreases with increasing applied bias. Magnitude of the contact resistances affects spin injection in the low bias regime as explained in Chapter 2 (figure 2.7).

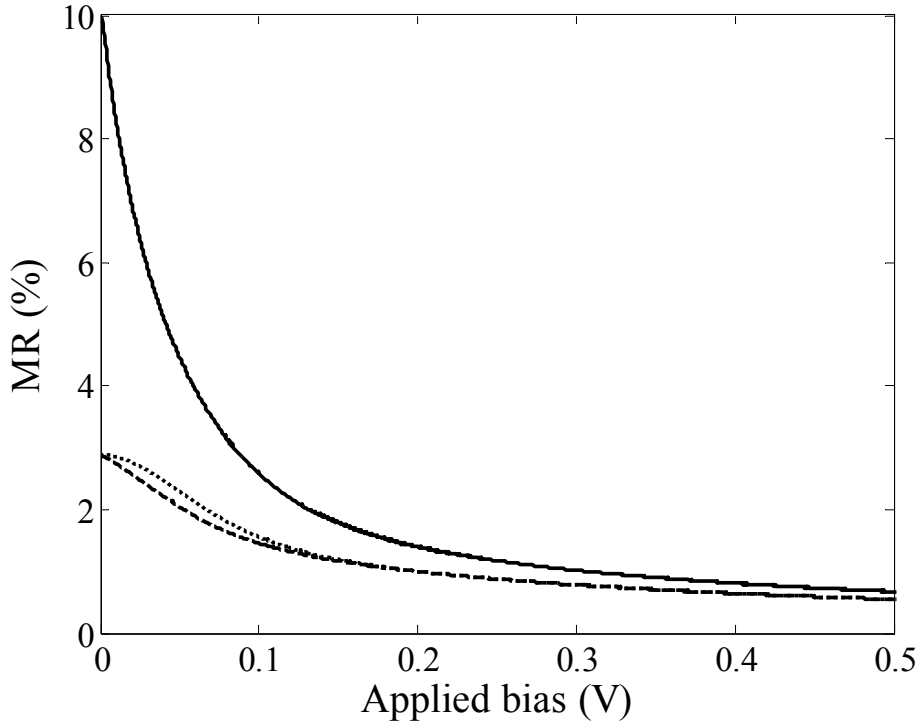

Figure 3.6. MR plotted as a function of the applied bias for the three cases as shown in figure 3.5.

3.5 Finite spin relaxation in the semiconductor

In steady state, the spin dependent carrier transport in the organic semiconductor is given by equations (3a) and (3b). It can be easily shown that the charge ($n = n_{\uparrow} + n_{\downarrow}$) and spin ($n_s = n_{\uparrow} - n_{\downarrow}$) continuity equations become,

$$\frac{d}{dx}\left(\mu n F + D\frac{dn}{dx} \right) = 0 \tag{3.8a}$$

$$\frac{d}{dx}\left(\mu n_s F + D\frac{dn_s}{dx}\right) - \frac{2n_s}{\tau_s} = 0 \tag{3.8b}$$

The spin continuity equation can be written in terms of spin diffusion length, L_{SD} ($=\sqrt{D\tau_s/2}$), as

$$\frac{d^2 n_s}{dx^2} + \frac{\mu F}{D}\frac{dn_s}{dx} - \frac{n_s}{L_{SD}^2} = 0 \tag{3.9}$$

The charge continuity equation, (3.8a) ensures that the charge current is constant throughout the device structure. The spin current depends on the position of the device due to finite spin relaxation in the semiconductor, and the spatial dependence of spin current is given by equation (3.9). The resulting spin density and spin current are

$$n_s(x) = Ae^{\lambda_1^{-1}x} + Be^{\lambda_2^{-1}x} \tag{3.10a}$$

$$j_s(x) = e\mu F\left(Ae^{\frac{x}{\lambda_1}} + Be^{\frac{x}{\lambda_2}}\right) + eD\left(\frac{A}{\lambda_1}e^{\frac{x}{\lambda_1}} + \frac{B}{\lambda_2}e^{\frac{x}{\lambda_2}}\right) \tag{3.10b}$$

Here, the constants A and B are determined from the boundary conditions; λ_1 and λ_2 are given by ($F < 0$)

$$\frac{1}{\lambda_1} = -\frac{eF}{2kT} + \sqrt{\left(\frac{eF}{2kT}\right)^2 + \frac{1}{L_{SD}^2}} \tag{3.11a}$$

$$\frac{1}{\lambda_2} = -\frac{eF}{2kT} - \sqrt{\left(\frac{eF}{2kT}\right)^2 + \frac{1}{L_{SD}^2}} \tag{3.11b}$$

Einstein's relation, $D/\mu = kT/e$ is used. A detailed description to determine the constants A and B using ohmic boundary conditions is given in Appendix A. Finally, we can express the charge current and the spin currents at the injecting and extracting contacts as follows

$$j = \frac{e\mu F N_0 \exp\left(-\frac{\Phi_B}{kT}\right)}{\exp\left(-\frac{eFL}{kT}\right) - 1}\left[\exp\left(-\frac{eFL}{kT}\right)\cosh\left(\frac{\Delta\mu(0)}{2kT}\right) - \cosh\left(\frac{\Delta\mu(L)}{2kT}\right)\right] \tag{3.12a}$$

$$j_s(0) = e\mu F N_0 \exp\left(-\frac{\Phi_B}{kT}\right)\left[P_0 \times \sinh\left(\frac{\Delta\mu(0)}{2kT}\right) - Q_0 \times \sinh\left(\frac{\Delta\mu(L)}{2kT}\right)\right] \tag{3.12b}$$

$$j_s(L) = e\mu F N_0 \exp\left(-\frac{\Phi_B}{kT}\right)\left[P_L \times \sinh\left(\frac{\Delta\mu(0)}{2kT}\right) - Q_L \times \sinh\left(\frac{\Delta\mu(L)}{2kT}\right)\right] \tag{3.12c}$$

In order to reduce the complexity, we assume that the organic semiconductor is symmetric with respect to the injecting and extracting contacts, such that $\Phi_{B;l} = \Phi_{B:r} = \Phi_B$. We express the spin currents at the injecting (Eq. 3.12 b) and extracting (Eq. 3.12c) contacts in a similar form to the case with no spin relaxation given by equation (3.4b). The constants P_0, Q_0, P_L, and Q_L (as shown in Appendix A) are expressed in terms of the device parameters as,

$$P_0 = \frac{1}{2} + \sqrt{\frac{1}{4} + \left(\frac{kT}{eFL_{SD}}\right)^2} \times \frac{\exp(\lambda_1^{-1}L) + \exp(\lambda_2^{-1}L)}{\exp(\lambda_1^{-1}L) - \exp(\lambda_2^{-1}L)} \tag{3.13a}$$

$$Q_0 = \frac{\sqrt{1 + \left(2kT / eFL_{SD}\right)^2}}{\exp(\lambda_1^{-1}L) - \exp(\lambda_2^{-1}L)} \tag{3.13b}$$

$$P_L = \sqrt{1 + \left(\frac{2kT}{eFL_{SD}}\right)^2} \times \frac{\exp\left(-\frac{eFL}{kT}\right)}{\exp(\lambda_1^{-1}L) - \exp(\lambda_2^{-1}L)} \tag{3.13c}$$

$$Q_L = \sqrt{\frac{1}{4} + \left(\frac{kT}{eFL_{SD}}\right)^2} \times \frac{\exp(\lambda_1^{-1}L) + \exp(\lambda_2^{-1}L)}{\exp(\lambda_1^{-1}L) - \exp(\lambda_2^{-1}L)} - \frac{1}{2} \tag{3.13d}$$

The charge current does not depend on spin relaxation in the semiconductor. Hence, the charge current expression Eq. (3.12a) is exactly the same as the earlier expression, Eq. (3.4a) with no spin relaxation. However, the spin currents at the injecting and extracting contacts, Eqs. (3.12b) and (3.12c), differ from that of Eq. (3.4b) due to finite spin relaxation in the semiconductor. It can be easily shown that in the limit of $L_{SD} \to \infty$ (no spin relaxation in the semiconductor) Eqs. (3.12b) and (3.12c) reduce to the previous result (Eq. 3.4b). The differences of the quasi-Fermi level at the injecting and extracting contacts are given by equation (3.1a) and (3.1b), respectively. Equations (3.1a), (3.1b), and (3.12a)-(3.12c) are solved self-consistently for an applied field, F, in the semiconductor and the applied bias across the device is calculated using equation (3.6), and finally the MR is calculated using equation (3.7).

3.6 Results with spin relaxation

We use the same device structure as discussed in section 3.5, but we consider only the bias dependent contact resistance of the form discussed above, $r_{\uparrow\downarrow}(\delta V) = r_{\uparrow\downarrow}(0)\exp(-\delta V / kT)$. The values of the SU and SD contact resistances at zero bias are 1×10^{-1} Ωcm^2 and 2×10^{-1} Ωcm^2 such that the ratio at zero bias, $r_{\uparrow}(0)/r_{\downarrow}(0)$ is ½. We also assume that the contact resistances are symmetric for the left and right contacts such that $r_l(0) = r_r(0)$. We plot the spatial dependence of spin polarization for various degrees of spin relaxation in figures 3.7 and 3.8 for P and AP configurations respectively.

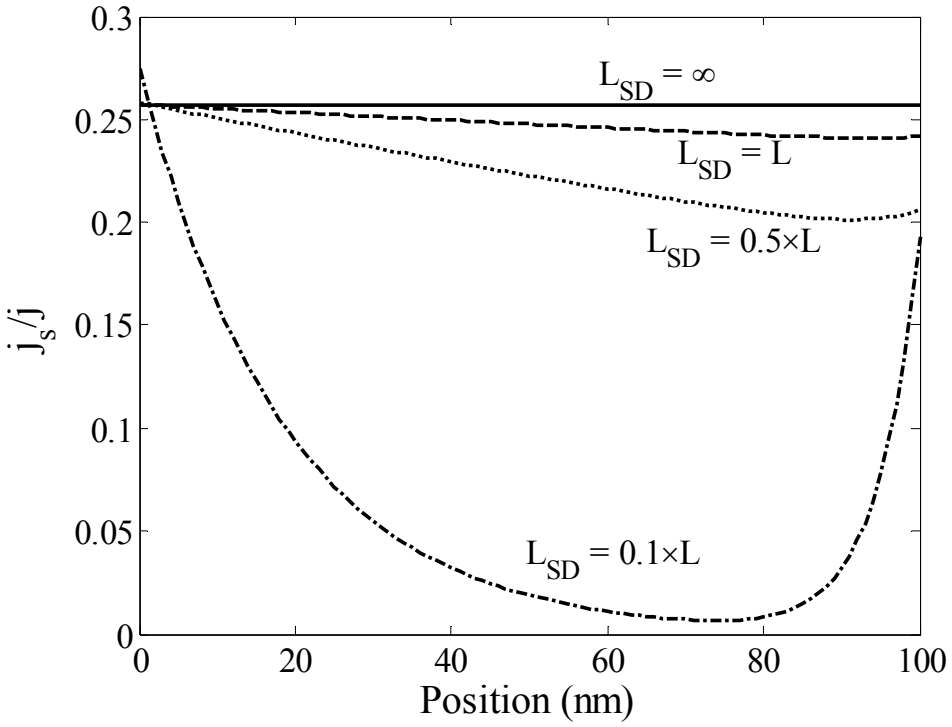

Figure 3.7. Spatial dependence of spin polarization, j_s/j, for P configuration. The spin diffusion lengths are shown in the figure and the applied bias is 0.5 V for all cases.

The applied bias across the device is 0.5 V for all cases shown. Spin injection, $j_s(0)/j$, depends on the injecting contact and identical for the P and AP contact magnetization. Spin polarization, j_s/j, decreases from the injecting contact towards the extracting contact due to spin relaxation inside the organic semiconductor. The rate of decrease depends on the spin diffusion length. The spin polarization completely depolarizes inside the organic semiconductor for a spin diffusion length of one tenth of the device thickness as evident from figures 3.7 and 3.8.

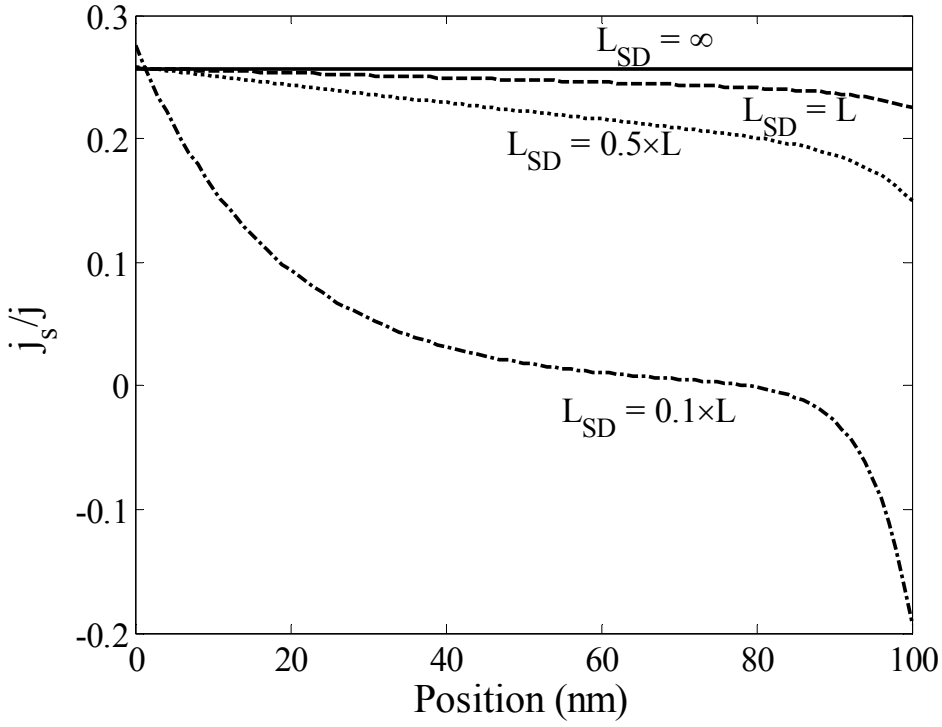

Figure 3.8. Spatial dependence of spin polarization, j_s/j, for AP configuration. The spin diffusion lengths are same as of P configuration and the applied bias is also 0.5 V for all cases.

However, the contact magnetization at the extracting contact is different for P and AP cases. As a result, spin polarization at the extracting contact is different for P and AP configurations. Spin polarization of the injected carrier density, n_s/n, is plotted in figure 3.9. In the case of parallel configuration, the quasi-Fermi levels of SU and SD electrons have to cross inside the organic semiconductor. Hence, spin polarization of the injected carrier density is positive at the injecting contact and negative at the extracting contact. For anti-parallel configuration, the quasi-Fermi levels do not cross and n_s/n is positive both at the injecting and extracting contacts. The effect of strong spin relaxation (L_{SD} = 0.1×L) results vanishing spin carrier density inside the organic semiconductor.

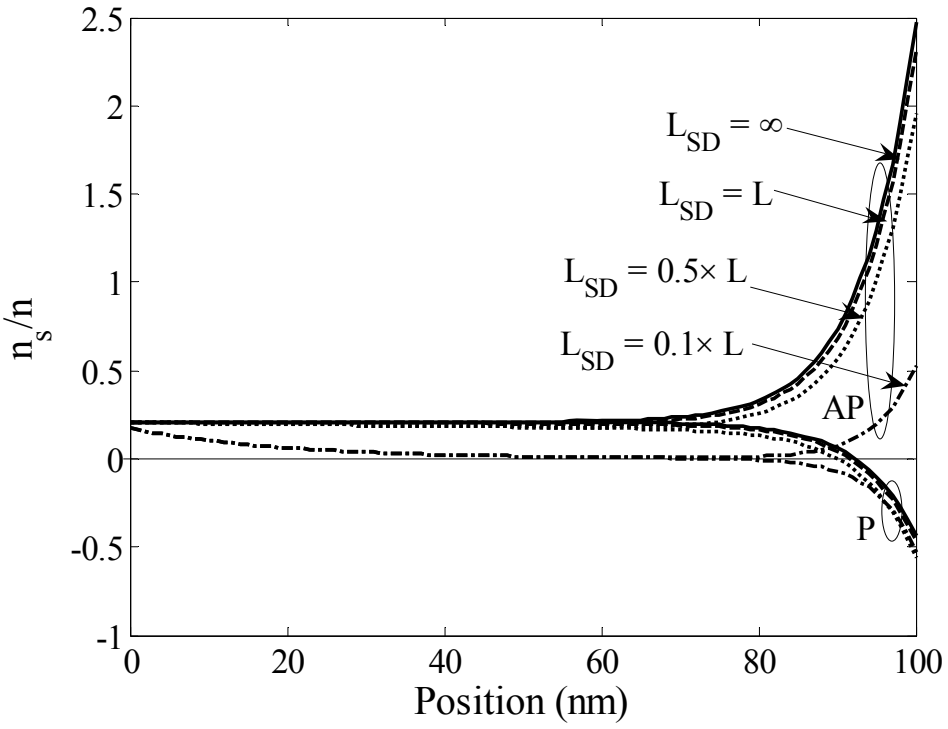

Figure 3.9. Spin polarization of the injected carrier density, n_s/n, plotted as a function of position of the device structure for different cases shown in figures 3.7 and 3.8.

We then explore how the spin relaxation inside the semiconductor affects the MR. The MR is plotted as a function of the applied bias in figure 3.10 for various degrees of spin relaxation as discussed in figures 3.7 – 3.9. The MR decreases with the applied bias for a given spin diffusion length. However, the MR strongly depends on the spin diffusion length of the semiconductor. For a spin diffusion length equal to the device thickness, the zero bias MR drops from 10% (value with no spin relaxation) to 2.5%. As the spin diffusion length becomes one tenth of the device thickness, the MR essentially vanishes.

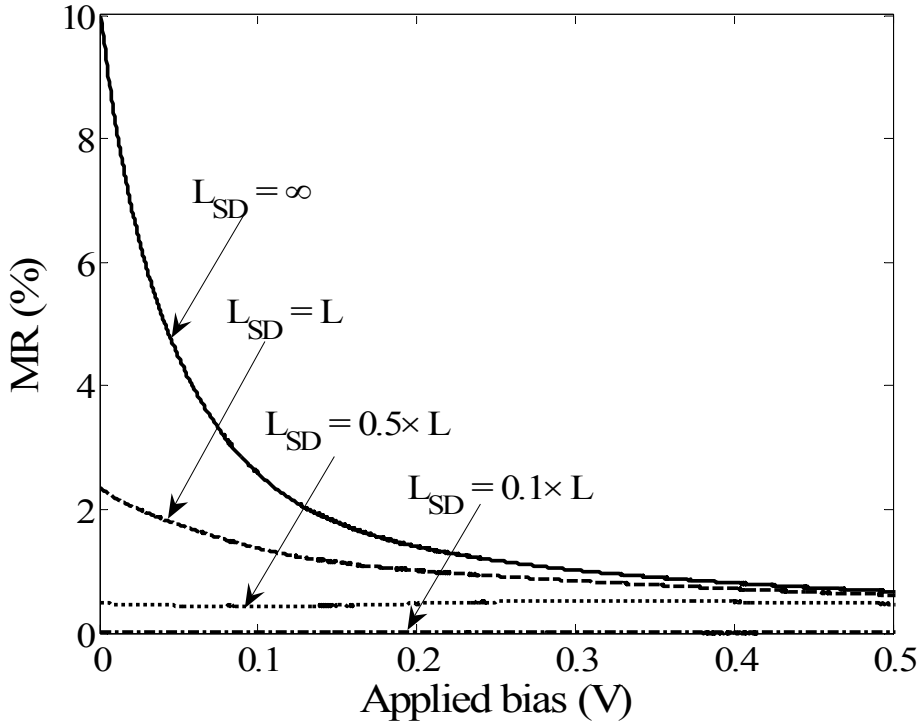

Figure 3.10. MR plotted as a function of applied bias across the device for the different spin diffusion lengths shown in figures 3.7 – 3.9.

Finally, we explore how the MR changes with device thickness in figure 3.11. The spin diffusion length is kept fixed at 200 nm for all cases. For each plot, the applied bias is also kept fixed. For a particular applied bias, the MR decreases exponentially with the device thickness. But the exponential coefficient does not truly reflect the spin diffusion length. The coefficient also depends on the applied bias. As an example, the exponential coefficients are 170 nm for 20 mV, 180 nm for 50 mV and 204 nm for 100 mV. The differences in exponential coefficients are due to the bias dependent contact resistances. Although the exponential coefficient does not accurately measure the diffusion length, this coefficient can yield a rough estimation of the spin diffusion length.

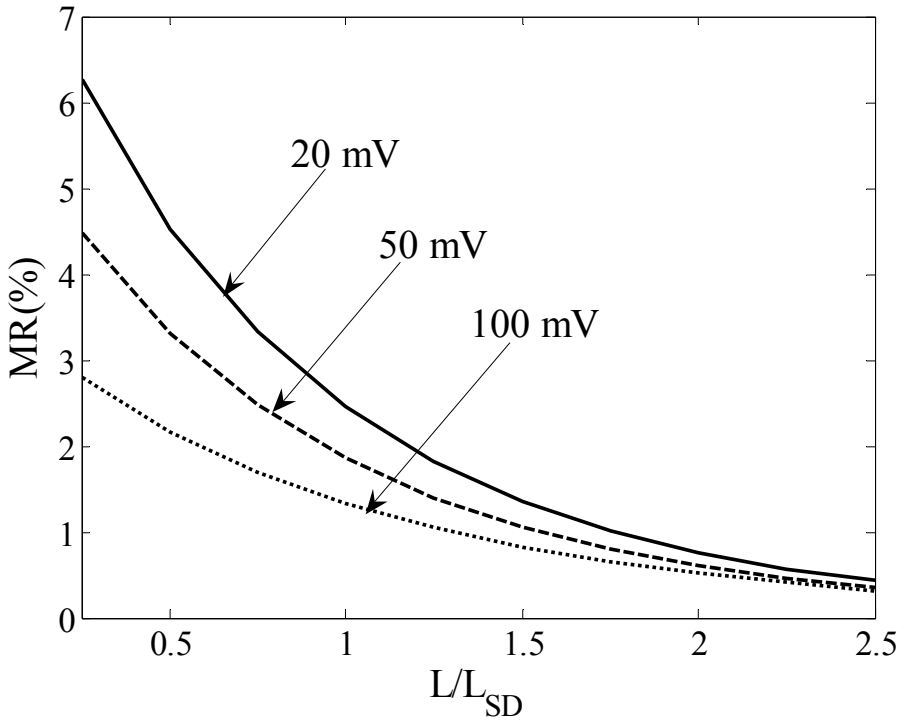

Figure 3.11. MR plotted as a function of device thickness for different applied biases. The spin diffusion length is kept fixed at 200 nm.

3.7 Conclusions

We can summarize these results for organic spin vales as follows: at low bias, both the injecting and the extracting contact control the spin polarization such that the spin polarizations are different for P and AP configurations. At high bias spin polarizations are almost equal for P and AP configurations; only the injecting contact controls spin injection. Measurable magneto-resistance requires spin selective tunnel contacts for both the injecting and the extracting electrodes. If the spin selective effective contact resistances are linear, the low bias MR may increase or decrease with increasing bias, depending on their relative magnitudes. However, the increasing current densities imply increasing voltage drops across the contact tunnel barriers, which may result in their increased transmissivity or decreased effective contact resistance. This may limit MR only to low applied bias. Spin relaxation has a strong effect on the MR. As the diffusion length becomes comparable to or less than the device thickness, the MR decreases rapidly from its value without spin relaxation, and the exponential coefficient of the MR versus device thickness measures a rough estimate of the spin diffusion length.

Chapter 4

Spin injection and extraction by tunnelling

Spin injection into semiconductors is greatly enhanced if the injection mechanism is spin selective, such as is the case for tunnelling from FM contacts. Electron tunnelling from a FM metal through a potential barrier into an organic semiconductor is spin dependent because the spatial part of the electron wave function is different for majority and minority spin electrons. In a device model, this process may be described by spin dependent contact resistances. We modeled organic spin valves using spin dependent contact resistances in Chapter 3. However, truly physical modeling of spin injection and detection requires a different treatment of the injection and extraction process. In this chapter, we discuss spin injection and extraction by tunnelling through a thin insulating layer.

4.1 Device structures

A schematic device structure for our calculation is shown in figure 4.1(a) where a thin insulating tunnel barrier between the FM contact and the organic semiconductor is considered. In actual devices, tunnel injection may involve such an interfacial layer or the potential barrier at the FM metal/organic semiconductor may serve as the tunnel

barrier. The former case is somewhat simpler and we will therefore focus on it. The thickness of the insulating layer is d and barrier height is Φ. For this model, the coordinate parallel to the transport direction is denoted by z.

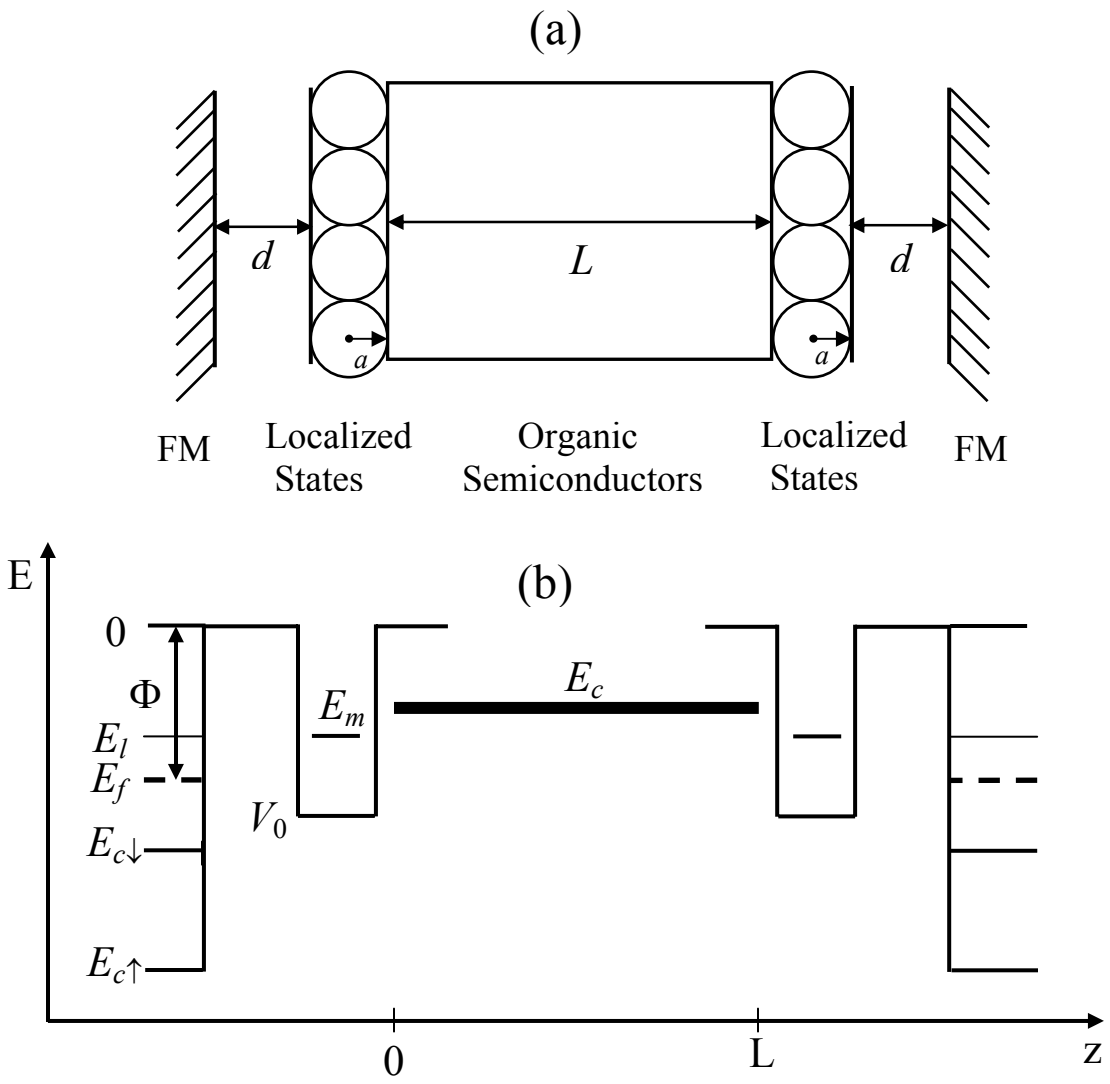

Figure 4.1. (a) Device structure for tunnel injection and extraction, (b) the corresponding schematic band diagram.

The region $0 < z < L$ corresponds to the bulk of the organic semiconductor where transport of injected charge carriers is diffusive. The schematic band diagram in equilibrium is shown in figure 4.1(b). E_l, E_f, and $E_{c\uparrow,\downarrow}$ are the energies of the tunnelling electrons, the Fermi energy, and the spin band edges of the FM contact, respectively. V_0, and a are the potential depth and radius of the molecular state, and E_m is its energy.

4.2 Tunnel injection/extraction model

Under suitable applied bias, electrons tunnel through the insulating layer into localized molecular states at the insulator/organic semiconductor interface. Subsequent transport in the semiconductor involves hopping of the injected electrons between neighboring molecules. Finally, the carriers are extracted by an analogous tunnelling process at the right contact. In many realistic cases, carrier injection from the FM contact into the organic semiconductor may in fact be due to positive charge carriers (holes), but this does not alter the results and conclusions reached in this work. (The possibility of tunnelling into localized states as an intermediate step in the injection of charge carriers into an inorganic semiconductor has been suggested previously).[57]

First, we consider tunnel injection at the left contact. Organic semiconductors usually display a strong degree of disorder; hence, there is no translational symmetry parallel to the metal/semiconductor interface. The tunnelling current between states

characterized by quantum numbers χ and ν can be calculated following the approach of Bardeen.[58,59,60]

$$I_t = 2\pi/\hbar \sum_{\chi,\nu} \left[f(E_l) - f(E_m + e\Delta V) \right] \left| T_{\chi\nu} \right|^2 \delta(E_l - E_m) \tag{4.1}$$

Here $f(E)$ is the Fermi Function, ΔV is the drop in the quasi-Fermi levels across the tunnel barrier and $T_{\chi\nu}$ is the tunnelling matrix element between states Ψ_χ of the left contact and localized molecular states Ψ_ν at the insulator/semiconductor interface. E_l and E_m are the energies of the states Ψ_χ and Ψ_ν, respectively. The tunnelling matrix element is calculated as,

$$T_{\chi\nu} = \left(\frac{\hbar^2}{2m_0} \right) \int d\vec{S} \bullet \left(\Psi_\chi{}^* \vec{\nabla} \Psi_\nu - \Psi_\nu \vec{\nabla} \Psi_\chi{}^* \right) \tag{4.2}$$

where the integral extends over the (x,y)-plane, and m_0 is the electron mass.

In the interest of keeping our discussion generic, we adopt a very simple model for the local molecular states, Ψ_ν. We take Ψ_ν to be the ground state wave function of a spherically symmetric potential well of radius a and potential depth V_0. It is convenient to choose the coordinate origin at the center of the potential well for the calculation of the tunnelling matrix element. The wave function for the localized molecular state outside the sphere is then given by:

$$\Psi_{\nu} = A\sin(k_r a)\exp(\kappa a)\frac{1}{r}e^{-\kappa r} \tag{4.3}$$

The pre-factor, $\sin(k_r a)\exp(\kappa a)$ arises from the matching condition at the boundary of the sphere and A is determined by normalization. Here,

$A^2 = 2/\left(a - \sin(2k_r a)/2k_r + \sin^2(k_r a)/\kappa\right)$, $k_r = \sqrt{2m_0(E_m - V_0)/\hbar^2}$, and

$\kappa = \sqrt{-2m_0 E_m/\hbar^2}$. The energy, E_m is calculated by solving the quantum well problem for a given choice of V_0.

The FM contact is spin polarized with the majority spin direction defined as the spin-up direction. The electrons in the FM contact are modeled as 'free', hence their bands are parabolic, and $E_{c\sigma}$, as shown in figure 1(b), are the band minima for the two spin directions. (σ is the spin quantum number: ↑ or ↓). The states of the FM contact are defined by four quantum numbers: l corresponds to the total energy, $\vec{k}_{\|}$ corresponds to the two parallel components of the wave vector, and σ to the spin. The wave function is a plane wave in the parallel direction and exponentially decaying inside the barrier. Thus, the relevant spatial wave function entering the tunnelling matrix element is given by,

$$\Psi_{\chi} = \frac{2ik_{l\sigma}}{ik_{l\sigma} - \alpha_l}\frac{e^{-\alpha_l(d+a)}}{(2\pi)^{3/2}}e^{-\alpha_l z}e^{-i\vec{k}_{\|}\cdot\vec{r}_{\|}} \tag{4.4}$$

Again the pre-factor, $2ik_{l\sigma}/(ik_{l\sigma} - \alpha_l)$ is determine from the matching conditions of the wave function at the FM/insulator interface and $e^{-\alpha_l(d+a)}/(2\pi)^{3/2}$ is due to normalization. Here, $k_{l\sigma} = \sqrt{2m_0(E_l - E_{c\sigma})/\hbar^2 - k_{\|}^2}$ and $\alpha_l = \sqrt{-2m_0E_l/\hbar^2 + k_{\|}^2}$.

In order to calculate the matrix element we expand the localized molecular wave function, Eq. 4.3, as:

$$\Psi_\nu = A'\int d^2q \frac{1}{2\pi}\frac{1}{\sqrt{q^2+\kappa^2}} e^{\sqrt{q^2+\kappa^2}\,z} \times e^{-i\vec{q}\cdot\vec{r}_{\|}} \tag{4.5}$$

Where $A' = A\sin(k_r a)\exp(\kappa a)$. Once the relevant wave functions are expressed in the form of Eqs. (4.4) and (4.5), it is straight forward to evaluate the matrix element $T_{\chi\nu}$:

$$T_{\chi\nu} = \frac{4\pi A'}{(2\pi)^{2/3}}\frac{\hbar^2}{2m_0}\frac{2ik_{l\sigma}}{ik_{l\sigma} - \alpha_l} e^{-\sqrt{\kappa^2+k_{\|}^2}\,(d+a)} \tag{4.6}$$

By substituting $T_{\chi\nu}$ and changing the summation over quantum numbers χ into integrations over $\vec{k}_{\|}$ and the energy E_l, the tunnelling current for spin σ from a continuum of states of the FM contact into a single localized state is obtained:

$$I_{t\sigma} = \frac{8}{\hbar}\left(\frac{\hbar^2}{2m_0}\right)^2 \frac{A'^2}{-E_{c\sigma}}\int d^2k_{\|}\sqrt{2m_0(E_m - E_{c\sigma}) - k_{\|}^2}\; e^{-2\sqrt{-2m_0E_m/\hbar^2+k_{\|}^2}\,(d+a)}$$
$$\times\left[f(E_m) - f(E_m + e\Delta V_\sigma)\right] \tag{4.7}$$

The Fermi functions in this expression insure that (for relatively small ΔV_σ) only states with energies close to the Fermi level, E_f, are relevant. If the number of molecular states with energy E_m per unit area is N_m (for either spin direction), the tunnelling current (flux of electrons per unit area) can be expressed by a simple rate equation given by,

$$j_{t\sigma} = \frac{1}{t_\sigma}\left(n_{m0}^{(2)} - n_{m\sigma}^{(2)}\right) \tag{4.8}$$

Here $n_{m0}^{(2)}$ and $n_{m\sigma}^{(2)}$ are the equilibrium and non-equilibrium sheet carrier concentrations (for a given spin direction) populating the molecular states involved in the tunnelling process, and are equal to $f(E_m)N_m$ and $f(E_m+e\Delta V_\sigma)N_m$, respectively. The tunnelling rate, $1/t_\sigma$ can be written as:

$$\frac{1}{t_\sigma} = \frac{8}{\hbar}\left(\frac{\hbar^2}{2m_0}\right)^2 \frac{A'^2}{-E_{c\sigma}} \int d^2k_\parallel \sqrt{2m_0(E_m - E_{c\sigma}) - k_\parallel^2}\; e^{-2\sqrt{-2m_0E_m/\hbar^2 + k_\parallel^2}\,(d+a)} \tag{4.9}$$

After tunnelling into the states Ψ_ν the electrons hop under the influence of the electric field in the organic semiconductor to other molecules. In the non-degenerate limit, the initial process is described by relationship similar to eq. (4.8):

$$j_{\tau\sigma} = \frac{1}{\tau}\left(n_{m\sigma}^{(2)} - n_{m0}^{(2)}\frac{n_\sigma(0)}{n_0}\right) \tag{4.10}$$

n_0 and $n_\sigma(0)$ are the volume carrier concentrations beyond the first molecular monolayer (i.e. at $z = 0$, according to figure 4.1b) under equilibrium and bias conditions, respectively.

τ is a spin independent hopping time constant, which for $E_m < E_c$ is written as $(\bar{a}^2 / D)\exp((E_c - E_m)/kT)$; $\bar{a}$ is the average hopping distance, D is the diffusivity of the organic semiconductor and E_c is the mean energy of relevant conduction (LUMO) states. Equations (4.8) and (4.10) can be combined to yield the current in terms of the equilibrium and non-equilibrium carrier concentration at $z = 0$:

$$j_{\sigma l} = \frac{n_{m0l}^{(2)}}{t_{\sigma l} + \tau_l}\left(1 - \frac{n_{\sigma l}(0)}{n_{0l}}\right) \tag{4.11}$$

The quantities $n_{m0l}^{(2)}$, n_{0l}, $t_{\sigma l}$, and τ_l all are equilibrium quantities. The subscript l now signifies the left contact. Analogous arguments for the right contact yield the current in terms of the carrier density at z = L:

$$j_{\sigma r} = \frac{n_{m0r}^{(2)}}{t_{\sigma r} + \tau_r}\left(\frac{n_{\sigma r}(L)}{n_{0r}} - 1\right) \tag{4.12}$$

Here, the subscript r identifies the right contact. The corresponding equilibrium carrier concentrations for the organic semiconductor at $z = L$ and the localized molecular states are n_{0r} and $n_{m0r}^{(2)}$, respectively. The tunnelling and hopping time constants are $t_{\sigma r}$ and τ_r, respectively.

For a particular spin direction, the current inside the bulk organic semiconductor is well described by the macroscopic drift-diffusion approximation:

$$j_{\sigma s} = -n_\sigma \mu F - \mu \frac{kT}{e} \frac{dn_\sigma}{dz} \tag{4.13}$$

Here, F (< 0) is the electric field, μ is the carrier mobility, k is the Boltzmann's constant, and T is the temperature. In principle, F is to be determined through Poisson's equation given an injected charge carrier density distribution. In order to remain within our essentially analytical framework, we will consider only small injected charge carrier densities and treat the field as constant. If we furthermore consider spin relaxation to be negligible, the current $j_{\sigma s}$ for a particular spin direction σ is conserved in the semiconductor and given by:

$$j_{\sigma s} = -\mu F \frac{n_{\sigma l}(0)\exp(-eFL/kT) - n_{\sigma r}(L)}{\exp(-eFL/kT) - 1} \tag{4.14}$$

Under steady state conditions, the currents expressed by equations (4.11), (4.12), and (4.14) are equal. Equations (4.11) and (4.12) can be used to eliminate the non-equilibrium carrier concentrations $n_{\sigma l}(0)$ and $n_{\sigma r}(L)$ in equation (4.14). The resulting current for an applied field F in the semiconductor can be expressed as a function of equilibrium carrier concentrations and the time constants for the left and right contact:

$$j_\sigma = \frac{-\mu F\left(n_{0l}\exp(-eFL/kT) - n_{0r}\right)}{\exp(-eFL/kT) - 1 - \mu F\left(t_{\sigma l} + \tau_l\right)\frac{n_{0l}}{n_{m0l}^{(2)}}\exp(-eFL/kT) - \mu F\left(t_{\sigma r} + \tau_r\right)\frac{n_{0r}}{n_{m0r}^{(2)}}} \tag{4.15}$$

To minimize parameters in the results to be discussed below we assume a symmetric structure with respect to the left and right contacts such that $n_{0l} = n_{0r} = n_0$ and $n_{m0l}^{(2)} = n_{m0r}^{(2)} = n_{m0}^{(2)}$. Equation (4.15) then simplifies to:

$$j_\sigma = \frac{-\mu F n_0}{1 - \frac{\mu F}{\exp(-eFL/kT) - 1} \frac{n_0}{n_{m0}^{(2)}} \left[\left(t_{\sigma l} + \tau_l \right) \exp(-eFL/kT) + \left(t_{\sigma r} + \tau_r \right) \right]} \tag{4.16}$$

Once we calculate the time constants for the left and right contact, we can calculate the current for a particular spin direction using equation (4.16). The P and AP configurations in this model (equation 4.16) are expressed through the time constants $t_{\sigma r}$. As an example, in order to calculate the SU current, $j\uparrow$, $t_{\uparrow_r}$ is used for P configuration but $t_{\downarrow r}$ is used for AP configuration. For a given configuration (P or AP), the charge current, j, is given by $j\uparrow + j\downarrow$ and the spin current, j_s, by $j\uparrow - j\downarrow$. Thus the currents and total applied voltages ($F \times L$) for the two contact alignments are obtained as a function of the applied field, F, across the semiconductor. We define spin injection into the organic semiconductors as:

$$\frac{j_s}{j} = \frac{j_\uparrow - j_\downarrow}{j_\uparrow + j_\downarrow} \tag{4.17}$$

As we assume negligible spin relaxation within the structure, the current polarization, j_s/j, is constant throughout the device structure. Spin injection is strongly dependent on the

spin transmission of the tunnel barrier, as discussed in reference. [61] We define the spin transmission of the tunnel barrier as:

$$\mathrm{S}T = \frac{t_{\downarrow} - t_{\uparrow}}{t_{\downarrow} + t_{\uparrow}} \tag{4.18}$$

Finally, the MR as defined by Eq. (3.7) in Chapter 3 is calculated.

4.3 Results for tunnel injection/extraction

As a specific example, we consider tunnel layers (both left and right contacts) of 3 nm thickness sandwiched between the FM contacts and the organic semiconductor. We assume a 100nm thick semiconductor with a carrier mobility of 10^{-2}cm^2/Vs, equilibrium carrier concentration (n_0) of 2×10^{14}cm^{-3}, (two-dimensional) density of relevant molecular states (N_m) of 10^{12}cm^{-2}. (The radius of the quantum well used to calculate the localized states is 5Å). We also assume that the same FM contacts are used in the left and right contacts such that the characteristic time constants $t_{\sigma l}$ are equal to $t_{\sigma r}$.

First, we explore the effect of the energy level E_m of the localized molecular state on the time constants t_m and τ_m, where the subscript m is added to indicate a particular choice of energy level. We consider a simple metallic contact (no spin dependence) with the band minimum 2.0eV below the Fermi energy of the contact. We plot the time

constants for that contact in figure 4.2 as a function of the energy level of the molecular states. Tunnelling favors high energies, hence the tunnelling time constant increases with decreasing energy, E_m. As we increase the barrier height, tunnelling becomes more difficult and t_m is larger for higher barriers.

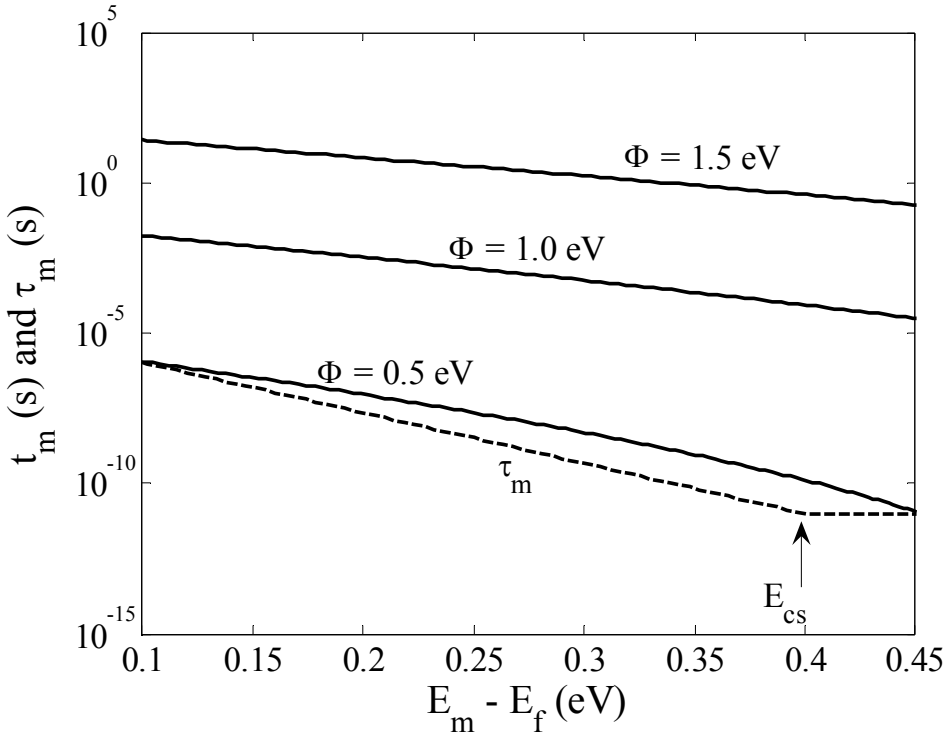

Figure 4.2. The time constants t_m (solid) and τ_m (dashed) plotted as functions of the localized molecular energy level with respect to the Fermi energy of the contact. The barrier thickness is 3nm and the barrier heights are shown in the figure.

On the other hand, the hopping time constant, τ_m does not depend on the barrier height. As we move down in the energy level with respect to the conduction band edge

E_c, the time to hop from the energy level to the conduction band increases, and for energy levels above E_c, τ_m becomes constant and equal to $\bar{a}^2 / D$. The hopping time constant, τ_m, can be comparable to the tunnelling time constant, t_m, depending on the barrier height and the barrier thickness. For a 3nm thick barrier, τ_m is comparable to t_m when the barrier height is 0.5eV.

The tunnelling current depends not only on the time constant t_m of a particular energy level but also on the probability of its occupation. Injection is balanced by a backflow. The quantity that determines the injecting tunnelling current is $f(E_m)/t_m$. We plot this forward tunnelling rate in figure 4.3 for the three cases shown in figure 4.2. The probability that a given energy level is occupied by a carrier decreases exponentially as the energy increases. As a result, the forward tunnelling rate increases as the energy level E_m decreases, i.e. relatively low energy molecular states are favoured if their occupation under non-equilibrium conditions is low.

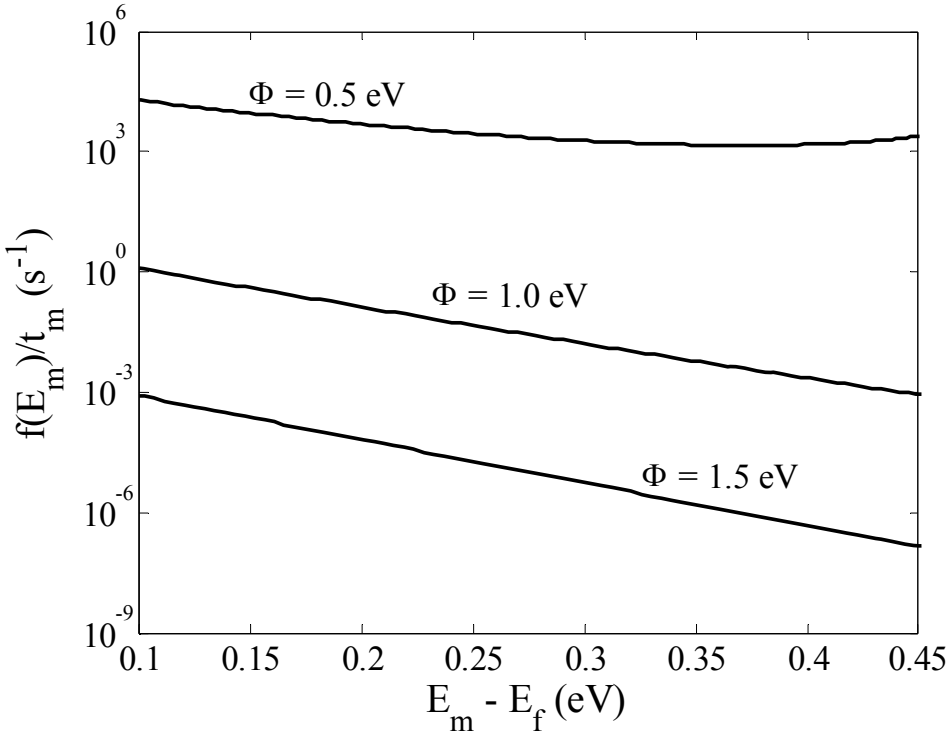

Figure 4.3. The forward tunnelling rate, $f(E_m)/t_m$, plotted for the three cases shown in figure 4.2.

We next plot the net tunnelling current for the three cases in figure 4.4. The applied field in the semiconductors for this case is 10^2 V/cm. Again the tunnelling current density generally decreases for increasing E_m. However, for the lowest energy barrier ($\Phi = 0.5$eV) the tunnelling rate is high. The rate at which the molecular states empty out ($1/\tau_m$) is comparable to the rate at which these states are occupied ($1/t_m$). Hence, the reduction of current with increasing E_m is not as strong as in the other two cases.

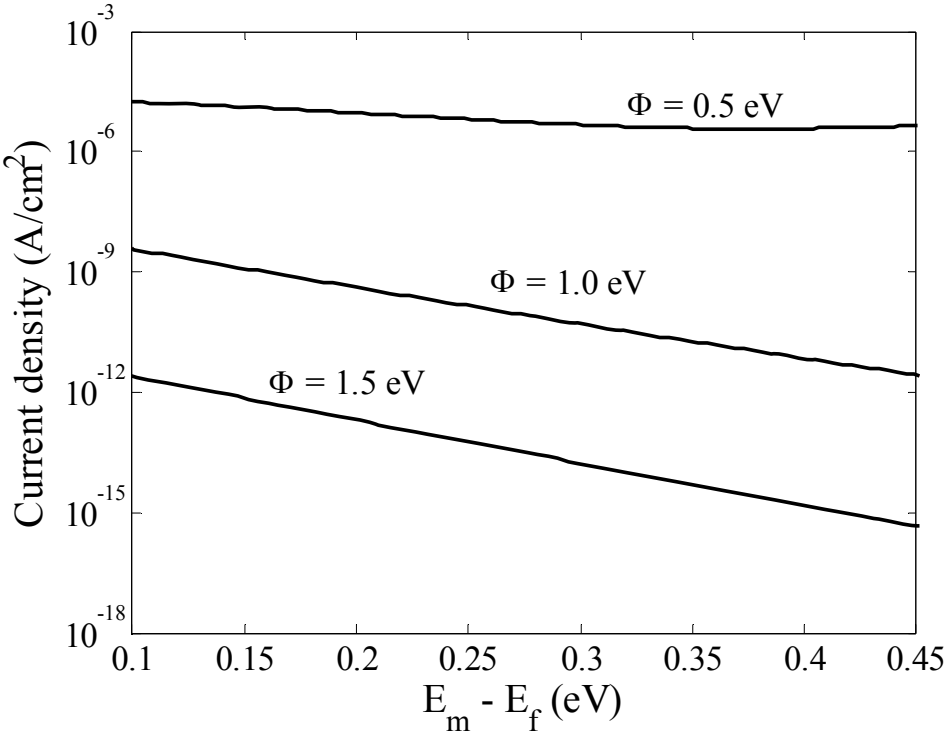

Figure 4.4. Net current density plotted for the three cases shown above. The applied field in the semiconductor is 10^2V/cm.

From these discussions we can conclude that molecular states of relatively low energy will contribute most to the tunnelling current. In real systems, there will typically be a relatively wide distribution of molecular energy levels available, but again in the interest of simplicity we will restrict our model to a single such level. For all calculations following we choose E_m to be 0.1eV above the equilibrium Fermi energy, and now we suppress the index m in the tunnelling and hopping time constants.

Tunnelling from a FM contact is spin dependent, because the tunnelling time constants t_σ are different for the majority and minority spin directions. The most

important quantity that determines the spin injection into the semiconductor is the spin transmission of the tunnel barrier. In figures 4.5 and 4.6, we plot the spin transmission (Eq. 4.18) as a function of molecular energy, E_m, and barrier height, Φ, respectively. The ratios of the Fermi wave vectors, $k_{f\uparrow}/\ k_{f\downarrow}$, have been determined for several relevant FM metals. [62] In terms of the energies, $E_{c\sigma}$, $k_{f\uparrow}/\ k_{f\downarrow} = \sqrt{(E_f - E_{c\uparrow})/(E_f - E_{c\downarrow})}$. (For figure 4.5, the energy levels are defined as $E_f - E_{c\uparrow} = 2.0$eV and $E_f - E_{c\downarrow} = 0.5$eV and for figure 4.6, the energy level $E_{c\downarrow}$ is fixed by taking $E_f - E_{c\downarrow} = 0.5$eV).

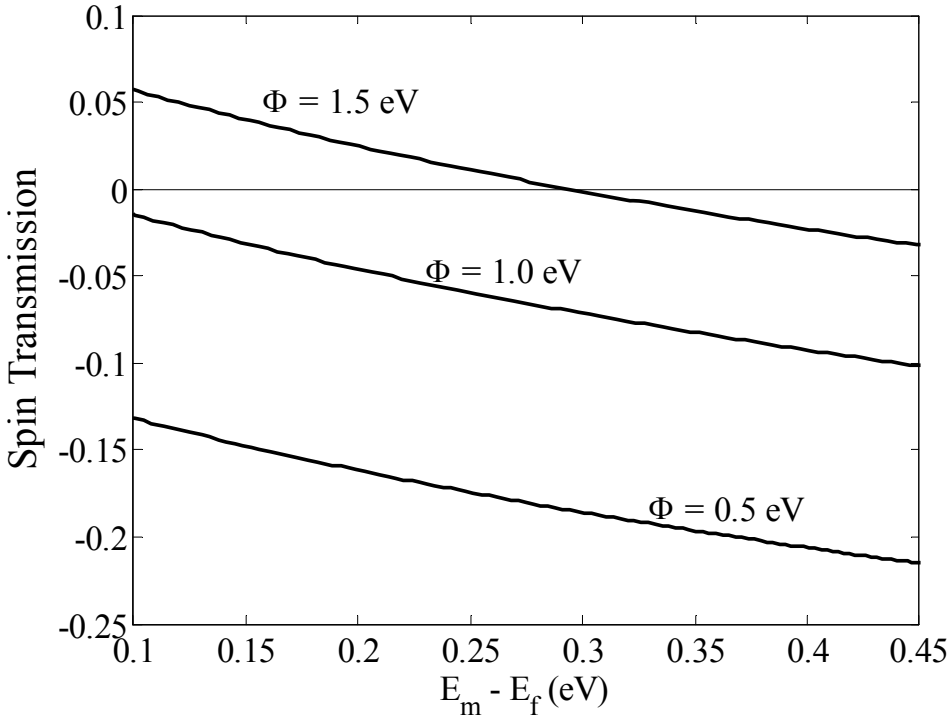

Figure 4.5. Spin transmission plotted as a function of E_m for three different barrier heights, $d = 3$nm, and $k_{f\uparrow}/\ k_{f\downarrow} = 2$.

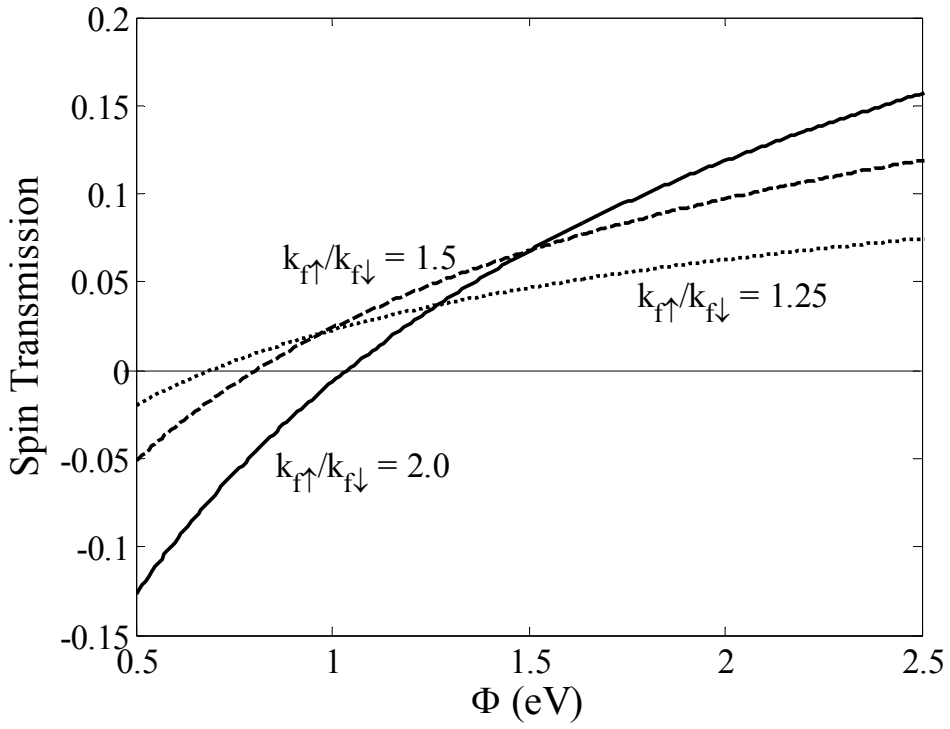

Figure 4.6. Spin transmission plotted as a function of the barrier height for different ratios of the Fermi wave vectors and d = 3nm.

The spin transmission is negative for low barriers and positive for large barriers and it can change sign between low energy molecular states and high energy molecular states. This arises from the non-monotonic dependence of the transmission coefficient on the incident state wave vector for fixed barrier height. Spin transmission tends to increase in magnitude as the ratio of the wave vectors increases.

We next compare the spin injection, j_s/j, with the spin transmission. The spin transmission and spin injection as a function of applied field in the semiconductor are

plotted in figure 4.7 for barrier heights of 1.5eV and 0.5eV. The ratio of the Fermi wave vectors is: $k_{f\uparrow}/k_{f\downarrow} = 2$. The effect of the electric field on the barrier is neglected in the calculation. The spin transmission is plotted for the injecting (left) contact. Spin injection depends on the relative orientation of the two contact magnetizations. We plot the spin injection for both parallel (solid line) and anti-parallel (dashed line) configurations. For a barrier height of 1.5eV the spin transmission is positive. Spin injection for the P configuration follows the spin transmission over the range of applied fields examined. For this large barrier height, the tunnelling rate is low compared to the thermally activated hopping rate, and j_s/j is essentially equal to the spin transmission. However, spin injection for the AP configuration is quite different. In the low field limit, spin injection for AP polarization of the contacts tends to zero. It increases as we increase the applied field, and in the high field regime spin injection for the AP configuration tends to approach the spin injection for the P configuration. A trend of this kind of the spin injection for P and anti AP configurations has also been discussed previously. On the other hand for low tunnel barriers, the magnitude of spin injection for the P configuration is smaller than the spin transmission. Here, the spin transmission rate from the ferromagnetic contact into the localized molecular states is comparable to or greater than the hopping rate. Injection into the semiconductor is less dependent on spin, and the magnitude of spin injection is small. Spin injection for the AP configuration follows similar behavior as discussed above for a barrier height of 1.5eV.

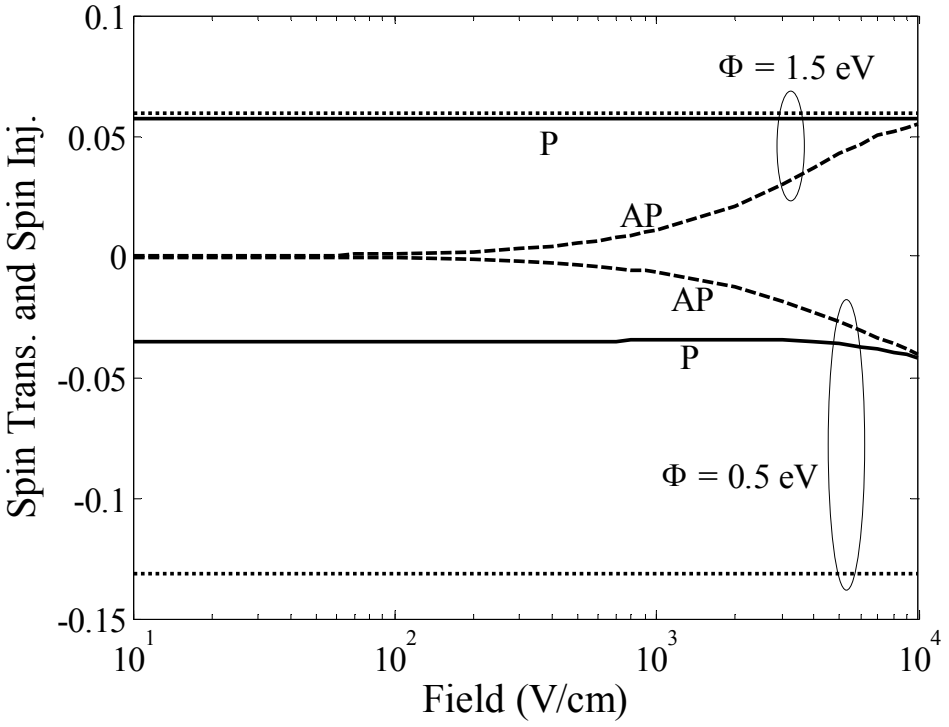

Figure 4.7. Spin transmission (dotted line) and spin injection (solid line for parallel and dashed line for anti parallel magnetization of the contacts) plotted as a function of applied field in the semiconductor. Barrier heights are 1.5eV and 0.5eV. For the case of P configuration and Φ = 1.5eV the dotted and solid curves coincide but have been offset slightly for clarity.

We next investigate the dependence of spin transmission and spin injection on the thickness of the barrier. In figure 4.8, we plot the spin transmission and spin injection as a function of the thickness of the barrier for barrier heights of 1.5eV and 0.5eV. The applied field in the semiconductor is 10^2 V/cm. We plot the spin injection only for the P

configuration. The spin injection for AP configuration is negligible in the low field region as shown in figure 4.7. Again the spin transmission is negative for barrier height 0.5eV and its magnitude decreases as the thickness of the barrier decreases. For a barrier height of 1.5eV, spin transmission is positive and increases as we decrease the thickness of the barrier. Hence, thin barriers favor spin transmission.

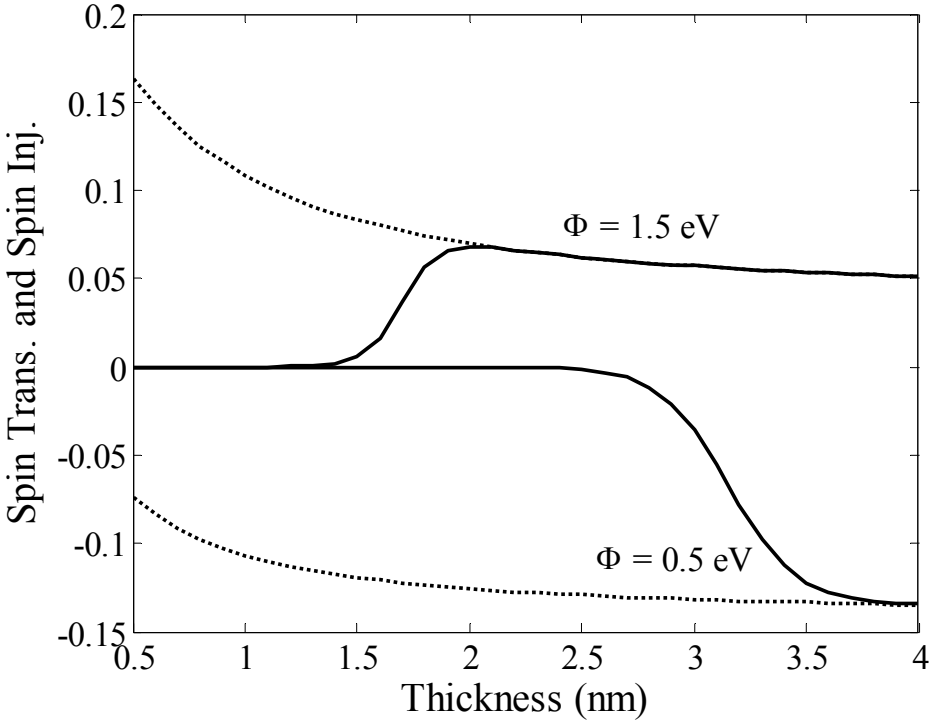

Figure 4.8. Spin transmission (dotted line) and spin injection (solid line) plotted as a function of thickness of the tunnel barrier. The barrier heights are 1.5eV and 0.5eV and the applied field in the semiconductor is 10^2 V/cm.

However, spin injection diminishes in magnitude as the thickness of barrier decreases irrespective of the barrier heights. For thin barriers, the tunnelling rate (from FM contact into localized molecules) is high compared to the hopping rate (from the localized states into the 'bulk' semiconductor), hence spin-polarization cannot be transferred effectively into the semiconductor and a thicker barrier is needed to achieve significant current polarization.

Next, we investigate the effects of tunnel injection and extraction on the MR. Again, the left and right contacts are symmetric such that the tunnelling time constants are equal i.e $t_{\uparrow l} = t_{\uparrow r}$ and $t_{\downarrow l} = t_{\downarrow r}$ for P configuration and $t_{\uparrow l} = t_{\downarrow r}$ and $t_{\downarrow l} = t_{\uparrow r}$ for AP configuration. We plot the MR and spin polarization as a function of the applied bias across the device in figures 4.9 and 4.10, respectively. The MR depends on the ratio of $t_{\downarrow} / t_{\uparrow}$. As the ratio of $t_{\downarrow} / t_{\uparrow}$ increases, spin injection and, hence, MR increases. However, the most striking point is the strong decrease of the MR with increasing applied bias for a fixed ratio of $t_{\downarrow} / t_{\uparrow}$ consistent with the experimental results. The decrease of the MR is due to the non-linearity of the injecting and extracting contacts. In the low bias regime, both contacts control the current and its spin polarization. Hence, the spin polarization and the charge current are different for P and AP configuration. The difference in charge current gives rise to MR effects. As the applied bias increases, the injecting contact exercises dominant control and the effect of the extracting contact diminishes. Hence, the spin polarization and charge current are equal for both configurations leading to vanishing MR.

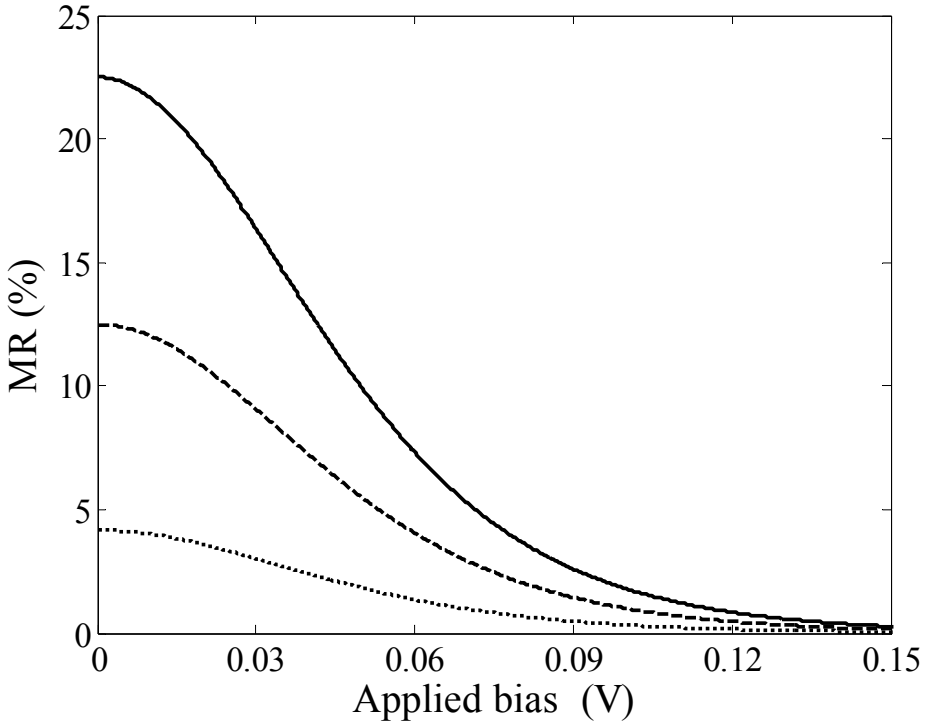

Figure 4.9. MR plotted as a function of applied bias across the device. The tunnel contacts at the injecting and extracting electrodes are symmetric with respect to spin injection. The ratio of the tunnelling time constants, $t_{\downarrow l}/t_{\uparrow l} = t_{\downarrow r}/t_{\uparrow r}$ for P ($t_{\downarrow l}/t_{\uparrow l} = t_{\uparrow r}/t_{\downarrow r}$ for AP) are 1.5 for the dotted line, 2.0 for the dashed line and 2.5 for the solid line.

In figures 4.5 and 4.6, we discussed that spin transmission for a tunnel junction can be positive or negative. It depends on the FM contact and the energy level of the molecular state involved in the injection process. For two different FM contacts at the injecting and extracting contacts, it is possible that the spin transmission is positive for one tunnel junction and negative for the other.

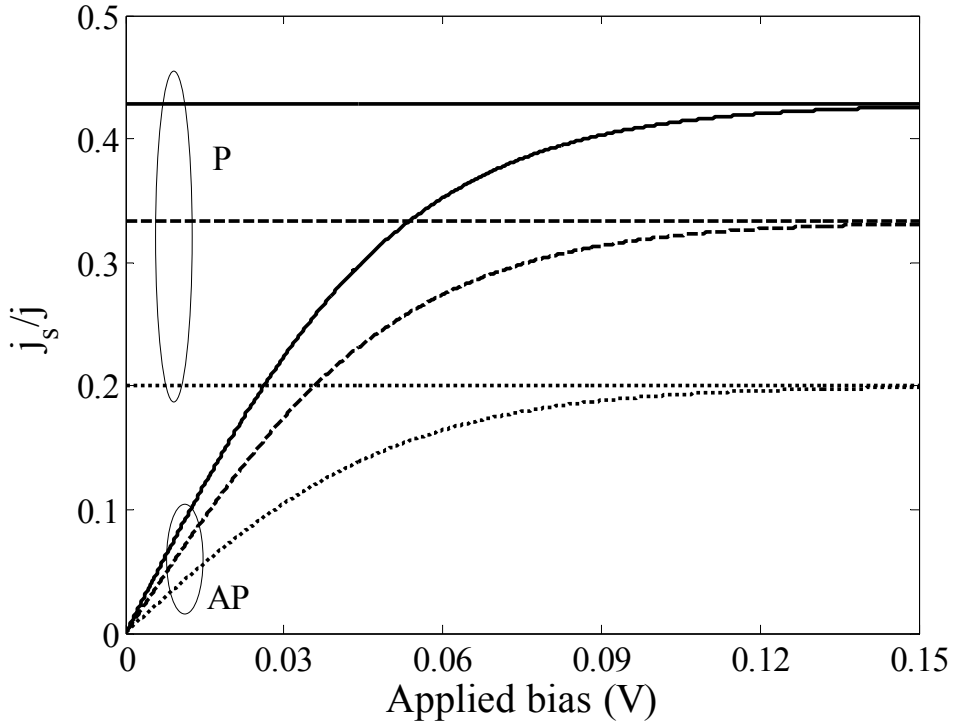

Figure 4.10. Spin polarization, j_s/j, plotted as a function of applied bias across the device for the three cases shown in figure 4.9.

In figure 4.11, we investigate the effect of asymmetric tunnel contacts on MR. We assume that the left contact is more transparent for majority (SU) electrons ($t_\uparrow < t_\downarrow$), but the minority carriers are favored by the right contact ($t_\downarrow < t_\uparrow$). We plot the MR in figure 4.11 for this type of device structure. The calculated MR is negative and its magnitude decreases strongly with increasing applied bias. Hence, the negative MR observed in some of the experimental devices may be attributed to negative spin injection from one contact and positive spin injection from the other contact.

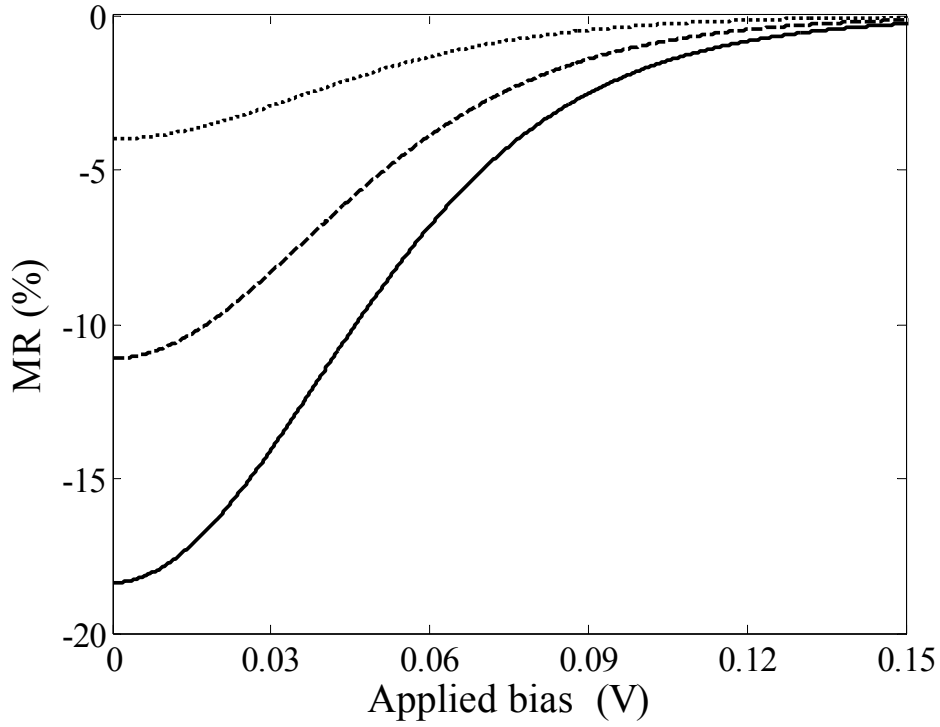

Figure 4.11. MR plotted as a function of applied bias across the device. The tunnel contacts at the injecting and extracting contacts are anti-symmetric with respect to spin injection. The ratio of the tunnelling time constants, $t_{\downarrow l}/t_{\uparrow l} = t_{\uparrow r}/t_{\downarrow r}$ for P ($t_{\downarrow l}/t_{\uparrow l} = t_{\downarrow r}/t_{\uparrow r}$ for AP) are 1.5 for the dotted line, 2.0 for the dashed line and 2.5 for the solid line.

4.4 Conclusions

Tunnelling from a FM contact provides a spin selective mechanism to inject spin polarized charge carriers into organic semiconductors. Localized molecular states close the contact and with energies in the vicinity of the equilibrium Fermi energy are the primary contributors to the tunnel current. The disordered nature of organic

semiconductors implies that such low energy states are more probable than in high quality inorganic semiconductor crystals. On the other hand, the low mobility of organic semiconductors tends to inhibit the effect of tunnel injection unless the tunnel rate is low. Spin transmission and, hence, spin injection strongly depend on the height of the barrier, the energy of the localized molecular states, and the Fermi wave vectors of the SU and SD electrons. Depending on the height of the barrier and the energy of the localized molecular states, spin injection through a tunnel barrier can be either positive or negative. As the barrier becomes more transparent (either by decreasing the barrier height or by decreasing the thickness of the barrier), spin injection decreases. A relatively thick barrier can efficiently transfer the spin into the semiconductors and the maximum spin injection is solely determined by the spin transmission of the barrier. The experimental observation of positive and negative MR may be attributed to the symmetry of the tunnel contacts with respect to spin transmission. If the injecting and extracting tunnel contacts are symmetric, such that both are transparent to one spin direction, positive MR results. On the other hand, one tunnel contact with positive spin transmission and the other tunnel contact with negative spin transmission results negative MR. The decrease of the MR with applied bias is due to the fact that with increasing applied bias, the injecting contact is taking control of the tunnel injection and charge and spin current become independent of the extracting contact.

Chapter 5

Summary and suggestions of future work

Spin injection, transport, and detection in organic semiconductors have been studied. The summary of this work and recommendations for future study are presented in this section.

5.1 Summary

The large conductivity mismatch between FM metal contacts and organic semiconductors hinders spin injection from the contacts into the semiconductors. For a spin polarized FM metal/semiconductor junction, the electrons in the metal and in the semiconductor are in good thermal contact, therefore the electrons in the semiconductor also stay in local quasi-thermal equilibrium. As a result spin injection under bias is weak. The applied field in the semiconductor can increase spin injection but in order to produce significant spin density in the semiconductor an unrealistically high charge current density is needed. Within practical values for the injected charge current density, the spin current density remains orders magnitude smaller than the charge current density.

Spin injection from FM contacts into organic semiconductors can be greatly enhanced if the injection mechanism is spin selective, such as is the case for tunnelling from FM contacts. Electron tunnelling from a FM contact can have significant spin dependence because the spatial part of the electron wave function is different for majority and minority spin states near the Fermi surface. In the conventional model for semiconductor spin valves, this process is described by spin dependent contact resistances that are different for majority and minority spin electrons. At low bias, spin injection depends on the relative magnetic orientation of the injecting and extracting contacts, and therefore spin injection is different for P and AP configurations. At high bias, only the injecting contact controls spin injection and spin injection is essentially independent of the extracting contact. Spin dependent contact resistances at the injecting contact are sufficient to inject a spin current into the semiconductor, but measurable MR requires a spin selective contact resistance at the extracting contact also. If the spin selective contact resistances are linear, the low bias MR may increase or decrease with increasing bias, depending on their relative magnitudes. However, the increasing current densities imply increasing voltage drops across the contact tunnel barriers, which may result in their increased transmissivity or decreased effective contact resistances. This may limit measurable MR to low applied bias. Spin relaxation inside the semiconductor has a strong effect on MR. As the spin diffusion length becomes comparable to or less than the device thickness, the MR decreases strongly from its value without spin relaxation. The exponential coefficient of the MR versus device thickness provides a rough estimate of the spin diffusion length.

Modelling tunnelling from a FM contact into an organic semiconductor as a process that involves localized states near the contact shows that states with energies in the vicinity of the equilibrium Fermi energy are primary contributors to the tunnel current and, hence, to spin injection. Spin injection into organic semiconductors by tunnelling strongly depends on the tunnel barrier, the energy of the localized molecular states, and the Fermi wave vectors of the SU and SD electrons of the FM contact. Depending on the height of the barrier and the energy of the localized molecular states, spin injection through a tunnel barrier can be either positive or negative. Here, positive and negative refer to spin transmission with respect to the majority spin. For large barrier heights, tunnel barriers are more transparent to minority spin. Small barriers favor minority spins. The thickness of the tunnel barrier also plays a vital role in the spin transfer into the organic semiconductor. As the barrier becomes more transparent (decreasing thickness of the tunnel layer) spin injection into the semiconductor decreases. A relatively thick barrier can efficiently transfer the spin into the semiconductor and the maximum spin injection is solely determined by the spin transmission of the barrier.

For a spin valve, the spin polarization in the semiconductor depends on the relative alignment of the contact magnetizations. At low bias, both contacts control the spin current and the spin polarization is different for P and AP configurations. At high bias, essentially only the injecting contact controls the spin polarization in the semiconductor, which then is independent of extracting contact. The observation of both positive and negative MR can be attributed to the spin transmission symmetry of the injecting and extracting contacts. If both the injecting and extracting tunnel contacts are

transparent to one spin direction, positive MR results. On the other hand, one contact with positive spin transmission and the other with negative spin transmission results negative MR. The MR decreases strongly with the applied bias. The decrease of the MR with increasing applied bias is due to the fact that both contacts control carrier injection at low bias. Hence, any change in contact alignments is detectable by electrical measurements. As the applied bias increases, the injecting contact is taking control of injection and the charge current depends only on the injecting contact. As a result, a change in the magnetization direction at the extracting contact cannot be detected through MR measurements.

5.2 Suggestions for future work

Although the work done in this thesis can explain some of the experimental results, additional model development is needed to provide a comprehensive explanation of the data obtained by the various teams involved in research on organic semiconductor spin valves. The present work can be extended by incorporating the following effects:

For tunnel injection and extraction, we consider the spin relaxation inside the organic semiconductor to be negligible, such that the spin current is constant throughout the device. In actual devices, spin relaxation inside the organic semiconductors is finite. We solved the spin diffusion problem inside the organic semiconductor and applied it to a model of organic spin valves where the tunnel contacts were represented by spin

dependent contact resistances. We need to incorporate the spin diffusion problem inside the organic semiconductor into the tunnel injection/extraction model where the tunnel contacts are represented by spin dependent rate equations. Incorporating the spin diffusion problem into the tunnel injection/extraction implies that the MR results depend on the thickness of the device structure. It should be analyzed whether the exponential coefficient of the MR versus device thickness truly reflect the spin diffusion length in the organic semiconductor or whether it really partially accounts for contact phenomena.

In the tunnel injection/extraction model, we consider tunnelling from the FM contacts into localized states of a single energy level. The disordered nature of organic semiconductors implies localized states distributed over a range of energies. The tunnelling probability is different for states with different energies. The tunnel injection model presented here should be generalized to multiple localized states of different energies.

In real devices, tunnel injection may involve an insulating layer or the potential barrier at the FM metal/organic semiconductor may serve as the tunnel barrier. We modeled the former case. In the latter, the tunnelling distances differ from one state to another state. As a result the tunnelling time constant will be different for different states of the same energy. Tunnel modeling through such a potential barrier can be the subject of future work.

Finally, tunnelling depends on the Fermi wave vectors or the energy band minima of the tunnelling electrons. In our calculation, we consider only simple free-electron-like bands, but generalizations are possible in principle and will be necessary to explain the peculiarities if specific FM contacts.

Lastly, it will be critical to incorporate effects associated with the applied bias into the tunnel injection model. These effects are likely to explain the charge current vs. voltage characteristics measured for organic semiconductor spin valves, which were not addressed in the work presented here.

References:

[1] *Semiconducting Polymers* v 1&2, edited by G. Hadziioannou and G. G. Malliaras (WILEY-VCH Weinheim, 2007).

[2] R. H. Friend, R. W. Gymer, A. B. Holmes. J. H. Burroughes, R. N. Marks, C. Taliani, D. D. C. Bradley, D. A. D. Santos, J. L. Brédas, M. Löglund, and W. R. Salaneck, Nature **397**, 121 (1999).

[3] J. Shinar and R. Shinar, J. Phys. D: Appl. Phys. **41**, 133001 (2008).

[4] *Organic Photovoltaics* edited by C. J. Brabec, V. Dyakonov, U. Scherf (WILEY-VCH, Weinheim, 2008).

[5] H. E. Katz and J. Huang, Annu. Rev. Mater. Res. 39, 71 (2009).

[6] J. Daughton, J. Magn. Materials, **192**, 334 (1999)

[7] G. A. Prinz, Science **282**, 1660 (1998).

[8] J. Fabian, A. Matos-Abiague, C. Ertler, P. Stano, and I. Žutić, Acta Phy. Slov., 57, pp. 565-907 (2007).

[9] S. A. Wolf, D. D. Awschalom, R. A. Buhrman, J. M. Daughton, S. von Molnar, M. L. Roukes, A. Y. Chtchelkanova, and D. M. Treger, Science **294**, 1488 (2001).

[10] M. E. Flatte and B. Vignale, Appl. Phys. Lett., vol. 78, pp. 1273, 2001.

[11] S. Datta and B. Das, Appl. Phys. Lett., vol. 56, pp. 665, 1990.

[12] R. Fiederling, M. Kelm, G. Reuscher, W. Ossau, G. Schmidt, A. Waag, and L. W. Molenkamp, Nature, vol. 402, pp. 787, 1999.

[13] Y. Ohno, D. K. Young, B. Beschoten, F. Matsukura, H. Ohno, and D. D. Awschalom, Nature, vol. 402, pp. 790, 1999.

[14] P. Bruno, and J. Wunderlich, J. Appl. Phys. vol 84, pp.978, 1998.

[15] V. A. Dediu, L. E. Hueso, I. Bergenti, and C. Taliani, Nature materials, vol. 8, 707 (2009).

[16] W. J. M. Naber, S. Faez, and W. G. van Der Wiel, J Phys. D. vol 40, pp. R205 (2007).

[17] *Organic Spintronics* edite by Z. V. Vardeny, CRC press, 2010.

[18] G. Schmidt, D. Ferrand, L. W. Molenkamp, A. T. Filip, and B. J. van Wees, Phys. Rev. B **62**, R4790 (2000).

[19] E. I. Rashba, Phys. Rev. B **62**, R16267 (2000).

[20] D. L. Smith and R. N. Silver, Phys. Rev. B **64**, 045323 (2001).

[21] J. D. Albrecht and D. L. Smith, Phys. Rev. B 66, 113303 (2002).

[22] A. Fert and H. Jaffrès, Phys. Rev. B 64, 184420 (2001).

[23] H. Jaffrès and A. Fert, J. Appl. Phys. 91, 8111 (2002).

[24] Z. G. Yu and M. E. Flatté, Phys Rev. B **66**, 201202 (2002).

[25] Z. G. Yu and M. E. Flatté, Phys Rev. B **66**, 235302 (2002).

[26] A. T. Hanbicki, B. T. Jonker, G. Itskos, G. Kioseoglou, and A. Petrou, Appl. Phys. Lett. 80, 1240 (2002)

[27] A. T. Hanbicki, O. M. J. van't Erve, R. Magno, G. Kioseoglou, C. H. Li, B. T. Jonker, G. Itskos, R. Mallory, M. Yasar, and A. Petrou, Appl. Phys. Lett. 82, 4092 (2003)

[28] H. J. Zhu, M. Ramnsteiner, H. Kostial, M. Wassermeier, H. P. Schonherr, and K. H. Ploog, Phys. Rev. Lett., vol. 87, pp. 016601 (2001)

[29] C. Adelmann, X. Lou, J. Strand, C. J. Palmstrom, and P. A. Crowell, Phys. Rev. B 71, 121301 (2005)

[30] S. A. Crooker, M. Furis, X. Lou, C. Adelmann, D. L. Smith, C. J. Palmstrom, and P. A. Crowell, Science 309, 5744 (2005)

[31] X. Lou, C. Adelmann, S. A. Crooker, E. S. Garlid, J. Zhang, K. S. M. Reddy, S. D. Flexner, C. J. Palmstrom, and P. A. Crowell, Nature Physics 3, 197 (2007).

[32] B. T. Jonker, Proceedings of the IEEE, vol. 91, pp.727 (2003).

[33] P. S. Davids, I. H. Campbell, and D. L. Smith, J. Appl. Phys. **82**, 6319 (1997).

[34] I. H. Campbell and D. L. Smith, Solid State Physics, edited by H. Ehrenreich and F. Spaepen, Vol. 55 (Academic, New York, 2001).

[35] J. Rybicki and M. Wohlgenannt, Phys. Rev. B 79, 153202 (2009).

[36] Y. Sheng, T. D. Nguyen, G. Beeraraghavan, Ö. Mermer, M. Wohlgenannt, S. Qiu, and U. Scherf, Phys. Rev. B 74, 045213 (2006).

[37] P. A. Bobbert, T. D. Nguyen, F. W. A. van Oost, B. Koopmans, and M. Wohlgenannt, Phys. Rev. Lett. 99, 216801 (2007).

[38] S. Funaoka, I. Imae, N. Noma, and Y. Shirota, Synth. Met. 101, 600 (1999), T. Wangwijit, H. Sato, S. Tantayanon, Polym. Adv. Technol. 13, 25 (2002) .

[39] C. G. Yang, E. Ehrenfreund, and Z. V. Vardeny, Phys. Rev. Lett. 99, 157401 (2007).

[40] T. D. Nguyen, G. H. Markosian, F. Wang, L. Wokcik, X.G. Li, E. Ehrenfreund, and Z. Valy Vardeny, Nature mat. 9, 345 (2010).

[41] I. H. Campbell, S. Rubin, T. A. Zawodzinski, J. D. Kress, R. L. Martin, D. L. Smith, N. N. Barashkov, and J. P. Ferraris, Phys. Rev. B 54, 14321 (1996).

[42] I. H. Campbell, J. D. Kress, R. L. Martin, D. L. Smith, N. N. Barashkov, and J. P. Ferraris, Appl. Phys. Lett. 71,3528 (1997).

[43] V. Dediu, M. Murgia, F. C. Matacotta, C. Taliani, and S. Barbanera, Solid State Commun. **122**, 181 (2002).

[44] Z. H. Xiong, Di Wu, Z. Valy Vardeny, and J. Shi, Nature **427**, 821 (2004).

[45] F. J. Wang, C. G. Yang, Z. Valy Vardeny, and X. G. Li, Phys. Rev. B **75**, 245324 (2007) .

[46] V. Dediu, L. E. hueso, I. Bergenti, A. Riminucci, F. Borgatti, P. Graziosi, C. Newby, F. Casoli, M. P. De Jong, C Taliani, and Y. Zhan, Phys. Rev. B 78, 115203 (2008).

[47] S. Majumdar, H. Huhtinen, H. S. Majumdar, R. Laiho, and R. Österbacka, J. Appl. Phys. **104**, 033910 (2008).

[48] Y. Liu, S. M. Watson, T. Lee, J. M. Gorham, H. E. Katz, J. A. Borchers, H. D. Fairbrother, and D. H. Reich, Phys Rev. B **79**, 075312 (2009).

[49] P. P. Ruden and D. L. Smith, J. Appl. Phys. **95**, 4898 (2004).

[50] M. Yunus, P. P. Ruden, and D. L Smith, Appl. Phys. Lett. **93** 123312 (2008).

[51] J. S. Jiang, J. E. Pearson, and S. D. Bader, Phys. Rev. B **77**, 035303 (2008).

[52] P. C. van Son, H. van Kempen, and P. Wyder, Phys. Rev. Lett. **58**, 2271 (1978).

[53] D. L. Scharfetter and H. K. Gummel, I EEE Trans. Electron Devices 16, 64 (1969).

[54] M. Yunus, P. P. Ruden, and D. L Smith, J. Appl. Phys **103**, 103714 (2008).

[55] J. S. Moodera, T. S. Santos, and T. Nagahama, J. Phys.: Condens. Matter 19, 165202 (2007).

[56] M. Yunus, P. P. Ruden, and D. L Smith, Syn. Metals **160**, 204 (2010).

[57] M. Tran, H. Jaffrès, C. Deranlot, J.M. George, A. Fert, A. Miard, and A. Lemaître, Phy. Rev. Lett. 102, 036601 (2009).

[58] J. Bardeen, Phys. Rev. Lett. 6, 57 (1961).

[59] M. H. Cohen, L. M. Falicov, J. C. Phillips, Phys. Rev. Lett. 8, 316 (1962).

[60] J. Tersoff and Hamann, Phys. Rev. B. 31, 805 (1985).

[61] Yunus, P. P. Ruden, and D. L Smith, Appl. Phys. Lett. **97**, 223304 (2010).

[62] *Calculated electronic properties of metals*, edited by V. L. Moruzzi, J. F. Janak, A. R. Williams (Pergamon Press, New York, 1979).

Appendix A: Solution of spin diffusion equation

In this appendix, we present a detailed description of the solution of the spin diffusion equation and the resultant spin currents at the injecting and extracting contacts. The spin diffusion equation in the semiconductor is given by

$$\frac{d^2 n_s}{dx^2} + \frac{eF}{kT}\frac{dn_s}{dx} - \frac{n_s}{L_{SD}^2} = 0 \tag{A1}$$

Here $n_s = n_\uparrow - n_\downarrow$ is the spin concentration, F is the field in the semiconductor, L_{SD} is the spin diffusion length, k is the Boltzmann constant and T is the temperature. The solution for the spin diffusion equation is of the form

$$n_s(x) = Ae^{\lambda_1^{-1}x} + Be^{\lambda_2^{-1}x} \tag{A2}$$

Here

$$\lambda_1^{-1} = -\frac{eF}{2kT} + \sqrt{\left(\frac{eF}{2kT}\right)^2 + \frac{1}{L_{SD}^2}} \tag{A3}$$

$$\lambda_2^{-1} = -\frac{eF}{2kT} - \sqrt{\left(\frac{eF}{2kT}\right)^2 + \frac{1}{L_{SD}^2}} \tag{A4}$$

The constants A and B are determined from the boundary conditions. Applying the boundary conditions at the injecting and extracting contacts of the semiconductor we get

$$n_s(0) = A + B = N_0 e^{-\frac{\Phi_B}{kT}} \sinh\left(\frac{\Delta\mu(0)}{2kT}\right) \tag{A5}$$

$$n_s(L) = Ae^{\lambda_1^{-1}L} + Be^{\lambda_2^{-1}L} = N_0 e^{-\frac{\Phi_B}{kT}} \sinh\left(\frac{\Delta\mu(L)}{2kT}\right) \tag{A6}$$

Where N_0 is the effective density of states and Φ_B is the Schottky barrier height (symmetric for left and right contacts). $\Delta\mu(0)$ and $\Delta\mu(L)$ are the splittings of the quasi-Fermi levels at the injecting and extracting contacts, respectively, and L is the thickness of the semiconductor.

Equation (A5) and (A6) give us the values of A and B, which can be written as,

$$A = \frac{n_s(0)e^{\lambda_2^{-1}L} - n_s(L)}{e^{\lambda_2^{-1}L} - e^{\lambda_1^{-1}L}} \tag{A7}$$

$$B = \frac{n_s(L) - n_s(0)e^{\lambda_1^{-1}L}}{e^{\lambda_2^{-1}L} - e^{\lambda_1^{-1}L}} \tag{A8}$$

The spin concentration (Eq. A2) gives us the drift-diffusion approximation of the spin current as,

$$j_s(x) = \mu F\left(Ae^{\lambda_1^{-1}x} + Be^{\lambda_{21}^{-1}x}\right) + \frac{\mu kT}{e}\left(\frac{A}{\lambda_1}e^{\lambda_1^{-1}x} + \frac{B}{\lambda_2}e^{\lambda_2^{-1}x}\right) \tag{A9}$$

Hence the spin current at the injecting ($x = 0$) and extracting ($x = L$) contacts can written as

$$j_s(0) = \mu F\left(A + B\right) + \frac{\mu kT}{e}\left(\frac{A}{\lambda_1} + \frac{B}{\lambda_2}\right) \tag{A10}$$

$$j_s(L) = \mu F\left(Ae^{\lambda_1^{-1}L} + Be^{\lambda_2^{-1}L}\right) + \frac{\mu kT}{e}\left(\frac{A}{\lambda_1}e^{\lambda_1^{-1}L} + \frac{B}{\lambda_2}e^{\lambda_{21}^{-1}L}\right) \tag{A11}$$

After some mathematical manipulation, the spin currents at the injecting and extracting contacts can be written in the form

$$j_s(0) = \mu F n_s(0)\left[\frac{1}{2} + \sqrt{\frac{1}{4} + \left(\frac{kT}{eFL_{SD}}\right)^2}\,\frac{e^{\lambda_1^{-1}L} + e^{\lambda_2^{-1}L}}{e^{\lambda_1^{-1}L} - e^{\lambda_2^{-1}L}}\right] - \mu F n_s(L)\left[\frac{\sqrt{1 + \left(2kT / eFL_{SD}\right)^2}}{e^{\lambda_1^{-1}L} - e^{\lambda_2^{-1}L}}\right] \tag{A12}$$

$$j_s(L) = \mu F n_s(0)\left[\sqrt{1 + \left(\frac{2kT}{eFL_{SD}}\right)^2}\,\frac{e^{-eFL/kT}}{e^{\lambda_1^{-1}L} - e^{\lambda_2^{-1}L}}\right] - \mu F n_s(L)\left[\sqrt{\frac{1}{4} + \left(\frac{kT}{eFL_{SD}}\right)^2}\,\frac{e^{\lambda_1^{-1}L} + e^{\lambda_2^{-1}L}}{e^{\lambda_1^{-1}L} - e^{\lambda_2^{-1}L}} - \frac{1}{2}\right] \tag{A13}$$

Substitution equation (A5) and (A6) into equation (A12) and (A13), we can express the spin current at the injecting and extracting contacts in the form:

$$j_s(0) = e\mu F N_0 e^{-\frac{\Phi_B}{kT}}\left[P_0 \times \sinh\left(\frac{\Delta\mu(0)}{2kT}\right) - Q_0 \times \sinh\left(\frac{\Delta\mu(L)}{2kT}\right)\right] \tag{A14}$$

$$j_s(L) = e\mu F N_0 e^{-\frac{\Phi_B}{kT}}\left[P_L \times \sinh\left(\frac{\Delta\mu(0)}{2kT}\right) - Q_L \times \sinh\left(\frac{\Delta\mu(L)}{2kT}\right)\right] \tag{A15}$$

where the constants P_0, Q_0, P_L, and Q_L are written in terms of the device parameters as

$$P_0 = \frac{1}{2} + \sqrt{\frac{1}{4} + \left(\frac{kT}{eFL_{SD}}\right)^2} \times \frac{e^{\lambda_1^{-1}L} + e^{\lambda_2^{-1}L}}{e^{\lambda_1^{-1}L} - e^{\lambda_2^{-1}L}} \tag{A16}$$

$$Q_0 = \frac{\sqrt{1 + \left(2kT / eFL_{SD}\right)^2}}{e^{\lambda_1^{-1}L} - e^{\lambda_2^{-1}L}} \tag{A17}$$

$$P_L = \sqrt{1 + \left(\frac{2kT}{eFL_{SD}}\right)^2} \times \frac{e^{-\frac{eFL}{kT}}}{e^{\lambda_1^{-1}L} - e^{\lambda_2^{-1}L}} \tag{A18}$$

$$Q_L = \sqrt{\frac{1}{4} + \left(\frac{kT}{eFL_{SD}}\right)^2} \times \frac{e^{\lambda_1^{-1}L} + e^{\lambda_2^{-1}L}}{e^{\lambda_1^{-1}L} - e^{\lambda_2^{-1}L}} - \frac{1}{2} \tag{A19}$$